



Keratin nanoparticles and photodynamic therapy enhance the anticancer stem cells activity of salinomycin

Greta Avancini^{a,1}, Andrea Guerrini^{b,1}, Claudia Ferroni^b, Daniele Tedesco^b, Marco Ballestri^b, Marta Columbaro^c, Luca Menilli^a, Elena Reddi^a, Roberto Costa^a, Luigi Leanza^a, Greta Varchi^{b,*}, Francesca Moret^{a,**}

^a Department of Biology, University of Padova, Padova, Italy

^b Institute for Organic Synthesis and Photoreactivity, Italian National Research Council, Bologna, Italy

^c IRCCS Istituto Ortopedico Rizzoli, Bologna, Italy

ARTICLE INFO

Keywords:

Salinomycin
Keratin nanoparticle
Photodynamic therapy
Chlorin e6
Cancer stem cells
Zebrafish embryo

ABSTRACT

The high rates of aggressiveness, drug resistance and relapse of breast cancer (BC) are mainly attributed to the inability of conventional therapies to equally eradicate bulk differentiated cells and cancer stem cells (CSCs). To improve the effectiveness of BC treatments, we report the in-water synthesis of novel keratin-based nanoformulations, loaded with the CSC-specific drug salinomycin (SAL), the photosensitizer chlorin e6 (Ce6) and vitamin E acetate (SAL/Ce6@kVEs), which combine the capability of releasing SAL with the production of singlet oxygen upon light irradiation. *In vitro* experiments on BC cell lines and CSC-enriched mammospheres exposed to single or combined therapies showed that SAL/Ce6@kVEs determine synergistic cell killing, limit their self-renewal capacity and decrease the stemness potential by eradication of CSCs. *In vivo* experiments on zebrafish embryos confirmed the capacity of SAL nanoformulations to interfere with the Wnt/ β -catenin signaling pathway, which is dysregulated in BC, thus identifying a target for further translation into pre-clinical models.

1. Introduction

Breast cancer (BC) is the most common cancer in women, accounting for 30% of all diagnosed cancers; despite the marked improvement of treatments over the last few years, it still represents the second leading cause of cancer-related deaths in women [1]. Although surgery, radiotherapy and chemotherapy are very efficient in eradicating bulk BC cells, the selective targeting of cancer stem cell (CSC) sub-populations is still an unmet need in the development of new effective anti-BC therapies to avoid tumor recurrence and formation of distal metastases [2]. In particular, bone metastasis represents the most debilitating complication occurring in up to 70% of patients with advanced BC. CSCs are a critical, dormant subset within the tumor mass capable of perpetuating the tumor: growing evidence has shown that cancer is a hierarchically organized tissue where CSCs trigger the formation of more differentiated bulk tumor cells with lower proliferative potential [3,4]. CSCs share similar properties with normal stem cells, including the ability of self-

renewal and differentiation that give rise to heterogeneous cancer cells. Due to this similarity, CSCs are commonly characterized by the expression of surface markers associated with stemness, such as CD133, CD44, CD90, but no specific markers are currently known to identify CSC populations [3,5]. Their tumorigenic potential is also characterized by the enhanced ability to repopulate the original tumor when transplanted into immunodeficient mice even at low clonal density [6]. Therefore, the development of effective therapeutic strategies to eliminate CSCs in combination with traditional chemotherapy or other treatment modalities would favorably impact the cure of BC.

Selective CSC targeting with small molecules has recently drawn much attention. Two main strategies have been applied to this purpose: the screening of small molecules and the tailored development of molecules interfering with known biological pathways through which CSCs are known to evolve, including Wnt/ β -catenin, Notch and Hedgehog signaling [7]. However, drugs that target these pathways may inherently be toxic to the stem-cell niche [8,9]. Among those molecules, the

* Correspondence to: G. Varchi, Institute of Organic Synthesis and Photoreactivity, Italian National Research Council, Via P. Gobetti, 101, 40129 Bologna, Italy.

** Correspondence to: F. Moret, University of Padova, Department of Biology, Via Ugo Bassi 58/B, 35100 Padova, Italy.

E-mail addresses: greta.varchi@isof.cnr.it (G. Varchi), francesca.moret@unipd.it (F. Moret).

¹ These authors contributed equally.

monocarboxylic acid polyether salinomycin (SAL), which is mainly used in veterinary medicine as an antibiotic for treating Gram-positive bacteria and coccidiosis infections, was identified as a selective compound inhibiting drug-resistant tumor cells and CSCs [10–12]. The selectivity of SAL toward CSCs has been associated to its ionophoric properties able to induce apoptosis/ferroptosis [13], and to its amphiphilic behavior enabling the transport of alkali metals across lipophilic membranes. SAL was shown to inhibit Wnt/ β -catenin signaling in chronic lymphocytic leukemia cells [14], prostate and breast cancer cells [15], as well as to prevent tumorsphere formation in MCF-7 BC cells by targeting the Hedgehog signaling pathway [16]. Furthermore, SAL combined with traditional chemo- and immune-therapies can improve the therapeutic outcome for a variety of cancer types, including leukemia, colorectal, prostate, breast and pancreatic cancer [17,18]. However, the clinical application of SAL for cancer treatment has been significantly hampered by its low water solubility, systemic toxicity and unfavorable pharmacokinetics [19]. To this end, several papers have reported the use of nanotechnology, *i.e.* synthesis of nanoformulations, for the delivery of SAL [20], alone or in combination with other drugs [21,22], such as doxorubicin [23], docetaxel [24], paclitaxel [25] and others [26].

Few studies have reported on the use of photodynamic therapy (PDT) as a mean for eradicating both the bulk tumor cells and CSCs [27–29]. PDT is an effective, non-invasive treatment based on the use of a light-activated photosensitizer (PS) that, in the presence of molecular oxygen, generates reactive oxygen species (ROS, mainly singlet oxygen) that induce cancer cell damage, tumor blood vessels destruction, and stimulation of antitumor immunological responses [30,31]. However, one of the major PDT limitations is the uneven and inadequate penetration of light inside tissues at different depths, which hampers its capability to reach the whole tumor mass to completely remove both bulk tumor cells and CSCs. In this framework, the combination of PDT with a specific CSCs molecule, such as SAL, could bring significant improvement in the outcome of BC treatment.

Here, we propose the unprecedented use of keratin-based nanoparticles (kNPs) as carriers of SAL and the PS chlorin e6 (Ce6) for the combined treatment of BC. Keratin was specifically selected as the delivery vehicle due to its unique and well-documented advantages over other biomaterials for drug delivery purposes [32–35]. Keratin shows excellent biocompatibility and ease of functionalization thanks to the presence of a large number of functional groups; in addition, the presence of both hydrophobic and hydrophilic domains can be exploited for the accommodation of a wide range of drug classes. Pure, high-molecular-weight and water-soluble keratin can be obtained through tailored extraction methods starting from renewable sources [36], and several methods for preparing kNPs are available, including desolvation, self-assembling, gelation, and drug-induced aggregation [33,37–40].

For the present study, keratin extracted from raw wool was covalently functionalized with Ce6 using known NHS chemistry by exploiting the free carboxylic group of the photosensitizer [41], whereas SAL was incorporated during the formation of kNPs by adding vitamin E (VE) acetate as the aggregating agent. VE esters, such as VE acetate, succinate and polyethylene glycol-1000 succinate, have been shown to be more stable against oxidation and to effectively function as pharmaceutical solubilizers and food supplements [42,43]. Indeed, previous investigations reported that the presence of VE and/or its esters does not affect the PDT efficacy, conversely it has been demonstrated that under certain conditions, VE could even augment the overall anticancer effect [44,45].

In addition to the preparation of different SAL and SAL/Ce6 kNPs, we herein report the results on the *in vitro* cytotoxicity exerted by the combination of SAL and Ce6-PDT against both BC cells monolayers and 3D BCSC-enriched mammospheres. Preliminary *in vivo* results on the anti-stemness potential of our SAL/Ce6 formulations in zebrafish embryos are also described.

2. Experimental section

2.1. Materials

2.1.1. Chemicals for synthesis and characterization

SAL was purchased from Cayman Chemicals (USA) and used without further purification. Ce6 was purchased from Livchem Logistics GmbH (Germany) and checked for purity before use. HPLC-grade methanol was purchased from Carlo Erba (Italy). All other chemicals used for the extraction of keratin, the preparation of kNPs and the HPLC analysis on SAL release from kNPs were purchased from Sigma-Aldrich (Italy). Ultrapure water was produced using a Sartorius Arium Pro® system (Italy).

2.1.2. Cell lines

MCF-7 and MDA-MB-231 human BC cells were purchased from American Type Culture Collection (ATCC, Rockville, USA). The cells were grown in DMEM with Glutamax™ supplemented with 10% heat inactivated fetal bovine serum (FBS), 100 U/mL streptomycin, 100 μ g/mL penicillin G and maintained at 37 °C under a humidified atmosphere containing 5% CO₂. Cell culture medium and supplements were purchased from Life Technologies (Italy), while sterile plasticwares were from Falcon® (Corning, USA).

2.2. Synthesis and characterization of kNPs

2.2.1. Keratin functionalization

Keratin was extracted from Merino wool by sulphitolysis as previously reported [41]. For the preparation of Ce6@kVE and SAL/Ce6@kVE kNPs, keratin was covalently functionalized with Ce6 as previously described [33,41]. Briefly, *N*-hydroxysuccinimide (NHS, 2 eq.) and 1-ethyl-3-(3-dimethylaminopropyl)-carbodiimide (EDC, 2 eq.) were added to a solution of Ce6 (1.0 eq.) in dimethyl sulfoxide (DMSO; 4.54 mM). The solution was then stirred in the dark at room temperature for 12 h to afford Ce6-NHS that was added to a solution of keratin (5 mg/mL) in sodium bicarbonate (NaHCO₃) buffer (0.1 M, pH 9.3). The initial Ce6/keratin ratio was 6% w/w (60 μ g_{Ce6}/mg_{keratin}). The mixture was stirred at room temperature and in the dark for 12 h, then transferred into a cellulose tube (molecular weight cut-off: 12–14 kDa) and dialyzed against milliQ H₂O, which was replaced with fresh one 3 times a day for 3 days. After dialysis, the purified functionalized ker-Ce6 solution was freeze-dried into powder. The extent of protein functionalization was assessed based on a previously collected standard calibration curve of free Ce6 (Fig. S1) and resulted to be in the 40 to 60 μ g/mg of protein range.

2.2.2. Preparation of SAL/Ce6@kVE and SAL@kVE kNPs

For the preparation of SAL/Ce6@kVE kNPs, an aqueous NaCl solution (0.9% w/v) was added to ker-Ce6 to have a final concentration of 8 mg/mL. The solution was vigorously stirred for 2–4 min and then sonicated until the complete dissolution of the protein. Stock solutions of VE acetate (30 mg/mL) and SAL (10 mg/mL) were prepared in ethanol. VE acetate and SAL stock solutions were then mixed in adequate proportions to obtain a solution with a VE acetate/SAL ratio of 2:3 w/w. The obtained VE acetate/SAL solution was slowly added via syringe to the keratin solution in adequate amount to obtain a VE acetate/keratin ratio of 8% w/w and a SAL/keratin ratio of 12% w/w; the mixture was then vigorously stirred for 1 h at room temperature in the dark, yielding monodisperse SAL/Ce6@kVE kNPs that were freeze-dried into powder. The preparation of SAL@kVE kNPs was achieved following an analogous procedure: an adequate volume of a 2:3 w/w VE acetate/SAL solution in ethanol was slowly added to a solution of pure keratin (8 mg/mL) in NaCl (0.9% w/v in water) to obtain a VE acetate/keratin ratio of 10% w/w a SAL/keratin ratio of 15% w/w; the mixture was stirred for 1 h at room temperature, affording monodisperse SAL@kVE kNPs that were freeze-dried into powder.

2.2.3. Preparation of SAL@ker, Ce6@kVE and Ce6@ker NPs

SAL (10 mg/mL in ethanol) was slowly added via syringe to keratin (8 mg/mL in aqueous NaCl 0.9% w/v) under vigorous stirring. The solution was stirred for 2 h affording SAL@ker kNPs. For the preparation of Ce6@kVE kNPs, ker-Ce6 was dissolved in NaCl (0.9% w/v in water) at a concentration of 8 mg/mL. VE acetate (30 mg/mL in ethanol) was then slowly added via syringe to the ker-Ce6 solution under vigorous stirring to a final VE acetate/keratin ratio of 9% w/w. A sudden opalescence indicated the formation of kNPs, which were freeze-dried after characterization of the particle size. Ce6@ker were prepared as previously described. [33]

2.2.4. Characterization of kNPs

The hydrodynamic diameter and polydispersity index (PDI) of kNPs in aqueous solution (0.5 mg/mL) was determined by dynamic light scattering (DLS) analysis at 25 °C using a NanoBrook Omni Particle Size Analyzer (Brookhaven Instruments Corporation, USA) equipped with a 35 mW red diode laser (nominal wavelength 640 nm). Electrophoretic mobility, *i.e.* zeta-potential, was measured at 25 °C using the same instrument. The stability of SAL/Ce6@kVE kNPs at 37 °C was evaluated over time (48 h) by measuring the hydrodynamic diameter and PDI on 0.5 mg/mL colloidal suspensions in phosphate buffer saline (PBS) and in a PBS/FBS (40:60, v/v) at predetermined time intervals. The morphology of kNPs was analyzed by transmission electron microscopy (TEM): SAL/Ce6@kVE kNPs (0.5 mg/mL) were dispensed as a drop on a carbon-coated nickel grid and allowed to dry for 1 h. For negative staining of samples, 10 µL of uranyl acetate solution (2% w/w in water) was added to the nickel grid and after 1 min any excess of the solution was absorbed by filter paper. The nanoformulation was subsequently observed with a Jeol Jem-1011 transmission electron microscope (Jeol Jem, USA).

2.2.5. Reactive oxygen species and singlet oxygen generation

The production of ROS was evaluated for SAL/Ce6@kVE, Ce6@kVE, and Ce6@ker using the chemical probe 2,7-dichlorodihydrofluorescein diacetate (H₂DCFDA). In details, H₂DCFDA was dissolved in methanol obtaining a 1.1 mM solution. 2 mL of NaOH (0.01 M) were then added to 500 µL to this solution and stirred for 30 min at room temperature; afterwards, 10 mL of phosphate buffer (pH = 7.4) were added providing the ROS probe solution. Subsequently, SAL/Ce6@kVE, Ce6@kVE and Ce6@ker kNPs in water were added (Ce6 final concentration 10 µM) to a cuvette containing milliQ water, 500 µL of phosphate buffer and 218 µL of ROS probe, as previously prepared. The solutions were irradiated with at 625 ± 20 nm with a red light (LED by Osram, Germany; 5 mW/cm²) up to 30 min and the absorbance spectra were recorded at each time point with an Eppendorf BioSpectrometer® basic, reading the peak increase at 500 nm.

Singlet oxygen generation was determined by the 9,10-dimethylanthracene (DMA) method. Quartz cells (0.75 mL) with a 1 cm path length and containing a solution of DMA (35 µM) in dimethylformamide (DMF) and SAL/Ce6@kVE, Ce6@kVE and Ce6@ker NPs (Ce6 final concentration 4 µg/mL) were irradiated at 625 ± 20 nm with a red light (Osram; power density 5 mW/cm²) for different irradiation times up to 300 s. The UV-Vis spectra were acquired in the 200–800 nm range and kinetics of DMA photo-oxidation were studied following the decrease of the absorbance at 378 nm.

2.2.6. SAL release kinetics from SAL/Ce6@kVE kNPs

SAL/Ce6@kVE kNPs (SAL content 1.05 mg) were suspended in 3 mL of buffer consisting of PBS 0.1 M (pH 6.8) and Tween-80 0.5% (w/v; PBS-T buffer) and dialyzed at 37 °C against 18 mL of the same solvent for 48 h using an MPM Instruments M 200-TBP incubator. 300 µL aliquots were sampled from the release medium at defined dialysis times (1, 2, 3, 4, 5, 7, 24 and 48 h) and replaced each time with an equal volume of fresh PBS-T.

Samples were then submitted to quantitative HPLC-UV analysis with

pre-column derivatization with 2,4-dinitrophenyl (DNP), which was carried out using a modified version of a previously published protocol: [46,47] (a) addition of methanol (50 µL); (b) addition of trichloroacetic acid (TCA) 50 mg/mL in water (50 µL); (c) sonication (10 min); (d) addition of DNP 1 mg/mL in methanol (100 µL); (e) incubation at 55 °C (20 min).

The analysis was performed on a Merck-Hitachi LaChrom HPLC system equipped with a L-7100 pump, a L-7400 UV detector, a D-7000 interface, a Rheodyne 7725i manual injection valve, and the DataApex Clarity Lite software; a Phenomenex Kinetex 5 µm C18 100 Å column, a methanol/(acetic acid 1.5% v/v in water) 94:6 v/v mobile phase, a 1 mL min⁻¹ flow rate, a 350 nm detection wavelength, and a 20 µL injection loop were used. SAL standards for calibration (2–100 µg/mL) were prepared by mixing aliquots of SAL 1 mg/mL in methanol (1–50 µL) with PBS-T (300 µL), and adjusting the volume to 350 µL with methanol, if necessary. All standards were processed according to pre-column derivatization steps (b)–(e) and submitted to HPLC-UV analysis in the same experimental conditions used for dialysis samples. The calibration curve was then derived by linear regression on HPLC peak areas plotted against SAL concentrations ($y = a + bx$), and the limit of quantification was determined from the ratio between the standard deviation of the intercept and the slope ($LOQ = 10s_a/b$).

The release kinetics and mechanism of SAL/Ce6@kVE kNPs was investigated by plotting the fraction of SAL content released from kNPs (f) against dialysis times (t). The early stage of release ($t \leq 3$ h) was analyzed by non-linear regression fitting using the Korsmeyer-Ritger-Peppas model ($f = k_{pl}t^n$) [48,49] to evaluate the release mechanism through the diffusional exponent n , while a first-order kinetics model ($f = a(1 - e^{-kt})$) was applied to the complete set of release data to estimate the half-time of the release ($t_{1/2} = \ln 2/k$).

2.3. In vitro experiments: mono-dimensional cell cultures

2.3.1. Uptake of Ce6@kVE kNPs in monolayered cancer cells

5×10^4 cells were grown in 24-well plates for 24 h and incubated for 48 h with 1 µM Ce6 as free drug or Ce6@kVE kNPs. At the end of the incubation time, cells were washed twice with Versene, detached from the plates with trypsin that was neutralized by the addition of FBS. Cells were centrifuged and resuspended in Versene before measuring Ce6 fluorescence using a BD FACSCanto™ II flow cytometer (Becton Dickinson, San Jose, USA). A blue laser (488 nm) was used to excite the PS and its fluorescence was detected at wavelengths > 670 nm (PerCP channel). For each sample, 10^4 events were acquired and analyzed using the FACSDiva software.

2.3.2. Cytotoxicity of SAL toward differentiated cancer cells

The cytotoxicity of SAL, either delivered as free drug or loaded into SAL@ker or SAL@kVE kNPs was measured with the MTS assay (CellTiter 96® Aqueous One Solution Cell Proliferation Assay, Promega Co., USA) in cells exposed to increasing SAL concentrations. 8×10^3 cells/well were seeded in 96-well plates, and after 24 h the medium was replaced with fresh one containing the drug delivered in free form or entrapped in kNPs. To evaluate SAL efficacy, cell viability was measured after 24, 48 or 72 h of drug incubation in the dark. For MTS assay cells were processed as previously reported [33]. Briefly, at the end of incubation time the medium was replaced with 100 µL of serum-free medium and 20 µL of the CellTiter 96® reagent. After 1 h, the absorbance at 492 nm was measured with a Multiskan Go (Thermo Fischer Scientific, USA) plate reader and cell viability was expressed as a function of absorbance relative to that of control cells (considered as 100% viability). Besides non-treated cells, an additional control was set with cells treated with sole VE acetate at the same concentration present in kNPs formulations.

2.3.3. Combination therapy and determination of combination index (CI)

For combination therapy experiments, cells were seeded as described above and treated with increasing concentrations of SAL, Ce6 or their

combination (Ce6/SAL ratio 1:1.8, w/w), delivered as free drugs or loaded into kNPs. Cells viability was measured 48 h after drug incubation in the dark (time point 48 h) as well as after an additional 24 h in which the cells were kept in drug-free medium (time point 48 + 24 h). For photo-toxicity experiments (PDT *in vitro*), cells were seeded and treated as described above, and at the end of the 48 h period, cells were washed twice with PBS Ca^{2+} and Mg^{2+} and irradiated with red light ($625 \text{ nm} \pm 20$) emitted by a OSLO LED lamp array (Osram, Germany), and with a total fluence of 20 J/cm^2 . The power density was 11.5 mW/cm^2 as measured with the radiometer PDT1200 (Waldmann, Germany). After irradiation and upon replacement of PBS with fresh medium, cells were incubated in the dark for 24 h prior the assessment of cells viability by MTS assay (phototoxicity; time point 48 h + 24 h). Furthermore, in order to determine if the combined treatment, e.g. SAL-chemotherapy and Ce6-PDT, resulted in a synergistic effect, CI values were calculated using the CompuSyn software (ComboSyn Inc., NJ, USA), and based on the Chou and Talalay method [50]. From the experimental data on cell viability, the Fraction affected (Fa) values were derived for each drug concentration and the data were processed by the CompuSyn software as described in [51]. For each drug and drugs combination, the software calculated also the drug concentration that inhibits cell survival by 50% (IC_{50} value).

2.3.4. ROS measurements in cells

A ROS detection Kit (Thermo Fisher Scientific, Waltham, MA, USA) was used for the assay. 4×10^4 cells were grown for 24 h in a 24-well plate, and treated with $1 \mu\text{M}$ Ce6, $1.4 \mu\text{M}$ SAL or their combination delivered as free form or entrapped in kNPs. After 48 h of incubation, cells were washed twice with PBS Ca^{2+} and Mg^{2+} and irradiated with red light ($625 \text{ nm} \pm 20$) with a total fluence of 9 J/cm^2 . Cells were detached from plates with trypsin and transferred to FACS tube. To detect intracellular ROS levels, the cells were incubated with ROS Assay Stain solution for 60 min at 37°C . The fluorescence signal of the ROS probe was measured using a BDFACSCanto™ II flow cytometer on FITC channel. For each sample, 10^4 events were acquired and analyzed using the FACSDiva software.

2.3.5. LDH assay

8×10^3 cells were grown in 96-well plates and, after 24 h of growth, were treated with increasing concentration of SAL, Ce6 or their combination delivered as free form or entrapped in kNPs. After 48 h of incubation, cells were washed twice with PBS Ca^{2+} and Mg^{2+} and irradiated with a red light ($625 \text{ nm} \pm 20$) at a total fluence of 20 J/cm^2 and a power density of 11.5 mW/cm^2 . PBS was then removed and replaced with fresh medium. After 24 h, LDH released into culture medium and present in the cells was measured to calculate the percentage of LDH release [medium LDH / (medium LDH + cellular LDH) $\times 100$], using the colorimetric CytoTox 96 Non-Radioactive Cytotoxicity Assay (Promega Co, Madison, WI, USA). Cellular LDH was determined after cells were lysed using lysis solution.

2.3.6. Annexin/PI assay

Cells (4×10^4) were seeded in 24-well plates; after 24 h, cells were treated with SAL, Ce6, or SAL/Ce6 delivered as standard formulations or in kNPs. At the end of the incubation time (48 h), and after cell irradiation (20 J/cm^2) and release in drug-free medium for additional 24 h (phototoxicity, 48 + 24 h), cells were detached from the plates with trypsin, and collected in flow cytometry tubes, washed with PBS and centrifuged. Annexin V, previously diluted in binding buffer, was added to each tube, and the cells were incubated in the dark for 10 min at room temperature, washed with the binding buffer, and then propidium iodide (PI) ($20 \mu\text{g/mL}$) was added before performing flow cytometry analysis.

2.4. *In vitro* experiments: 3D cell cultures with CSC-enriched mammospheres

2.4.1. Generation and treatment of mammospheres

Mammospheres from MDA-MB-231 and MCF-7 adherent cells were generated as described in our previous study [29]. For assessing the effects of single and combined therapies toward mammosphere formation efficiency (MFE) two different treatment protocols were applied.

Protocol 1: cells were seeded and treated with drugs/irradiated in monolayer and, at the end of treatment interval, were re-seeded to form first generation mammospheres (1st generation). In details, cells (0.15×10^6) were seeded in 60 mm tissue culture dishes and 24 h later, treated for 48 h with the different drugs combinations. At the end of the incubation time, cells were irradiated in PBS (20 J/cm^2 of red light) and, immediately after irradiation, were detached from plates and re-seeded in ultra-low attachment plates (0.1×10^6 and 5×10^3 cells for MDA-MB-231 and MCF-7, respectively) to allow the formation of the 1st generation mammospheres. The number of formed mammospheres was evaluated by counting the number of spheres from images acquired by bright-field microscopy (DMI4000 Leica microscope, Germany). The mean diameter of each mammosphere was calculated with the LAS AF Lite software, and spheres with a diameter below $100 \mu\text{m}$ were excluded from counting. MFE was calculated as the number of spheres counted in the 1st generation, divided by the number of seeded cells, and expressed as percentage means \pm SD.

Protocol 2: mammospheres were formed as described above and incubated for 48 h with the drugs formulations directly in ultra-low attachment plates. At the end of the incubation time, the spheres were irradiated with 1 J/cm^2 of red light, when PDT was part of the treatment, and, immediately after irradiation, mammospheres were dissociated and re-seeded in non-adherent condition to allow the formation of second-generation (2nd generation) mammospheres, without changing the number of seeded cells with respect to 1st generation. MFE was calculated as the number of spheres counted in 2nd generation, divided by the number of cells seeded, and expressed as percentage (means \pm SD).

2.4.2. Aldehyde dehydrogenase (ALDH) activity assay

ALDH enzymatic activity in 2nd generation mammospheres was measured using ALDEFLUOR™ Kit (STEMCELL Technologies, Canada), following the manufacturer's protocol. Briefly, mammospheres were dissociated into single cells and then cells were re-suspended in Aldefluor Buffer and stained with activated Aldefluor Reagent. As control for background fluorescence, for each sample, $500 \mu\text{L}$ of cell suspension were transferred in a tube containing di-ethyl-amino-benzaldehyde (DEAB), a specific inhibitor of ALDH. After incubation for 40 min at 37°C , cells were centrifuged at $250 \times g$ for 5 min, re-suspended in $500 \mu\text{L}$ of Aldefluor Buffer, and analyzed with the flow cytometer.

2.4.3. Uptake of Ce6 in mammospheres

1st generation mammospheres were generated as described above and incubated for 48 h with $1 \mu\text{M}$ Ce6 loaded into kNPs or delivered as free drug. The localization of the PS was evaluated by confocal microscopy (Leica SP5) by transferring the mammospheres from 24-well/plates to 35 mm cell imaging dishes (Ibidi, Germany) and washing them twice with PBS before visualization. Images were acquired from the top to the bottom of the mammosphere in about 20 different focal planes (z-stack $10 \mu\text{m}$). Furthermore, a 3D reconstruction of the distribution of the fluorescence signal in the equatorial plane of the mammospheres was obtained using the software ImageJ and a maximum projection image obtained by superimposition of 20 focal plains using the software LAS AF Lite (Leica).

2.5. *In vivo* experiments: the zebrafish embryo model

Zebrafish (animals and embryos) were maintained according to

standard rules and procedures (<https://zfin.org>). All animal manipulation procedures were conducted according to the Local Ethical Committee at the University of Padua and National Agency (Italian Ministry of Health), and with the supervision of the Central Veterinary Service of the University of Padova (in compliance with Italian Law DL 116/92 and further modifications, embodying UE directive 86/609). Transgenic lines Tg(7xTCFX.lasiam:EGFP) and Tg(hsa.cox8a:mls-EGFP) also known as Tg(COXVIII-mls:EGFP) were previously reported [52,53], and manipulated accordingly. The lines are currently stabled at the zebrafish facility of Padua University. For the experiments, kNPs or SAL free solutions were either injected in the yolk or applied in the fish water. Microinjection is performed on randomly separated sibling embryos at 1 cell stage, adding ~ 0.05 pmol (~ 5 nL) of SAL in Danieau solution/egg (final concentration ~ 50 nM). Chorions were manually excised at 24 h post-fertilization (hpf) and images were acquired at 36 hpf. Zebrafish embryos expressing fluorescent proteins were analyzed using a Leica M165FC epifluorescent microscope, equipped with a Nikon DS-F12 digital camera. All images were acquired with the same exposure parameters and processed with GIMP 2.0.

3. Results and discussion

3.1. Synthesis and characterization of different kNPs

The combination of different drugs/therapies is widely recognized as a powerful strategy to increase the outcome of BC therapy, especially in terms of tumor recurrence control; however, specific treatments aimed at eliminating both differentiated cancer cells and CSCs have not been reported so far. Moreover, little is known on the use of PDT as treatment option against CSCs [28,29,54], as well as on its possible combination with CSC-specific repurposed drugs such as SAL. In order to combine Ce6-PDT with SAL while enhancing drug solubility and bioavailability, SAL/Ce6@kVE kNPs were prepared through the nanoprecipitation procedure, consisting in the slow addition of an ethanol solution of SAL to an aqueous saline solution of ker-Ce6 (Fig. 1A). The addition of properly defined percentages of VE acetate (5–15% $w_{(VE)}/w_{(kNPs)}$) during kNPs preparation was found to promote the formation of highly

stable and reproducible nanoparticles, avoiding the use of toxic aggregating or cross-linking agents. Through this procedure, SAL loading could be finely tuned from 5 to 25% $w_{(SAL)}/w_{(kNPs)}$.

SAL/Ce6@kVE kNPs were obtained with an average hydrodynamic diameter of 127 nm, depending on the preparation conditions, an average zeta potential of -27 mV and an average PDI of 0.13, indicating the presence of a single and highly monodisperse kNPs population (Tables S1 and S2). As expected, and as previously reported [41], the particles are provided with a negative zeta potential which is ascribed to the presence of the SO_3^- and the COO^- groups on the protein backbone. After lyophilization, kNPs were resuspended in PBS yielding a homogeneous colloidal suspension with an average hydrodynamic diameter of 130 nm (PDI = 0.21), showing that lyophilization is a reliable method for kNPs storage and subsequent reconstitution from powder.

TEM observations showed that SAL/Ce6@kVE kNPs were isolated, spherical in shape and with sizes in agreement with DLS results (Figs. 1B, S2).

SAL/Ce6@kVE kNPs showed negligible size variation and a limited increase in PDI (from 0.2 to 0.4) over 48 h in PBS at $37^\circ C$, suggesting a reasonable stability of SAL/Ce6@kVE kNPs under these conditions (Fig. S3). As expected, the hydrodynamic diameter of SAL/Ce6@kVE kNPs increased from 140 to 180 nm in the presence of FBS over the same observation time (Fig. S4), most likely due to the interaction between kNPs and serum proteins. Importantly, the change in size is within the acceptable range of variation and the presence of serum proteins does not induce the formation of aggregates, as confirmed by the constant PDI (0.2–0.3).

The release of SAL from SAL/Ce6@kVE kNPs was determined by a HPLC method with pre-column derivatization that allowed for analysis times below 10 min (SAL elution time: 4.7 min) and showed good linearity ($R^2 = 0.9991$) up to $100 \mu g/mL$; the resulting LOQ ($8.96 \mu g/mL$) was adequate to quantify SAL in all the analyzed samples.

The release of SAL from SAL/Ce6@kVE kNPs into the dialysis medium (PBS-T) already reached completion after 7 h (Fig. 1C). The diffusional exponent ($n = 0.639 \pm 0.046$) obtained by fitting the Korsmeyer-Ritger-Peppas model to the early stage of SAL release ($R^2 = 0.9929$) suggests that the release of SAL from kNPs is governed by non-

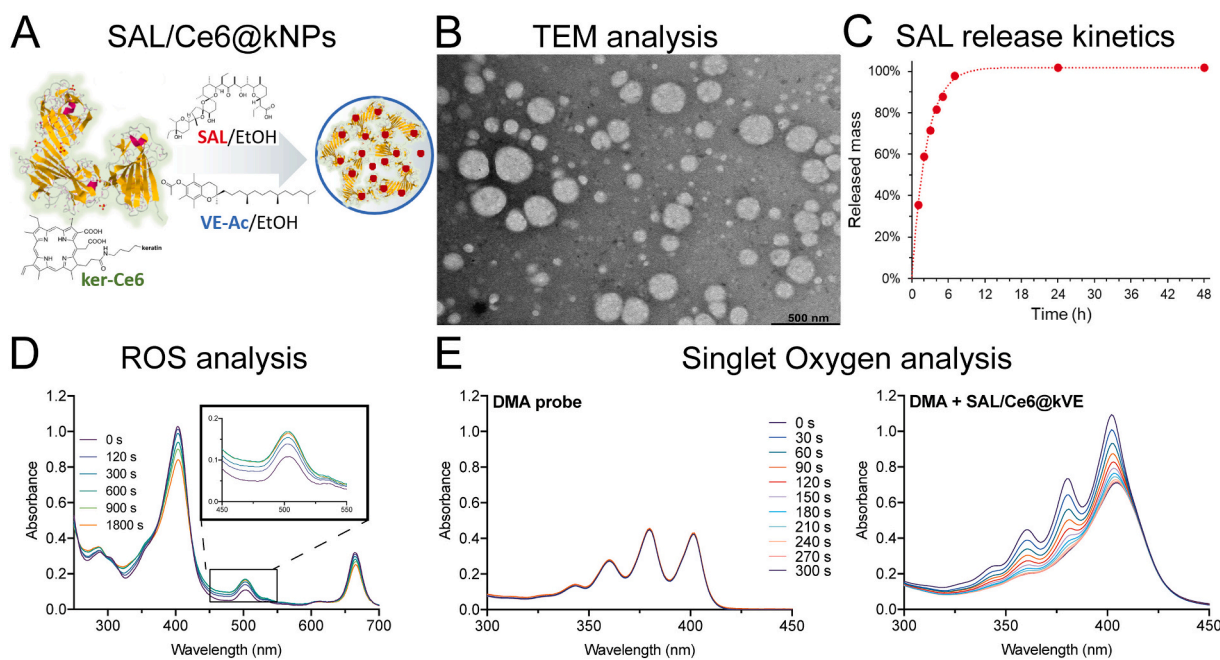


Fig. 1. SAL/Ce6@kVE kNPs characterization. (A) Schematic representation of SAL/Ce6@kVE kNPs preparation and structure. (B) Representative transmission electron microscope (TEM) image of SAL/Ce6@kVE kNPs. Scale bar represents 500 nm; magnification 60,000 \times . (C) SAL release kinetics. (D) ROS production analysis. (E) singlet oxygen analysis performed at different irradiation times of a solution of DMA alone and of DMA + SAL/Ce6@kVE kNPs.

Fickian diffusion; the application of a first-order kinetics model to the full set of data ($R^2 = 0.9976$) allows to predict a $t_{1/2}$ value of 1.66 h for the release.

Ce6@kVE, SAL@kVE and SAL@ker kNPs were prepared as control particles to compare the different treatment modalities. Ce6@kVE and SAL@kVE kNPs were obtained by nanoprecipitation using VE acetate as aggregating agent as previously described for SAL/Ce6@kVE kNPs. Ce6@kVE kNPs had an average hydrodynamic diameter of 168 nm (PDI = 0.26) (Table S3) and a negative zeta potential of -30 mV (Table S2), while SAL@kVE kNPs displayed a 154 nm diameter (PDI = 0.13) (Table S4) and a zeta potential of -27 mV (Table S2). In order to determine whether the presence of VE acetate had an effect on biological activity when combined with SAL into kNPs, SAL@ker kNPs were obtained by exploiting the hydrophobic interaction of SAL with the protein. This procedure afforded kNPs of 127 nm with a PDI of 0.4 (Table S5), and a negative zeta potential of -29 mV (Table S2). The greater PDI of SAL@ker kNPs is ascribed to the lower ability of SAL alone to induce stable kNPs aggregation.

The efficiency of PDT treatment is highly dependent on the amount of ROS produced and therefore the ROS generation efficiency of the PS loaded into SAL/Ce6@kVE kNPs was assessed by measuring the increase of 2,7-dichlorofluorescein (DCF) absorption peak at 500 nm. Indeed, the non-fluorescent H_2DCFDA is hydrolyzed and oxidized to highly fluorescent DCF in the presence of ROS. For this experiment, a solution of SAL/Ce6@kVE kNPs and ROS probe (see Experimental section) was irradiated with a LED red light (625 nm) and as shown in Fig. 1D, the DCF absorption at 500 nm increased proportionally with increasing the irradiation time. Thus, even when loaded into kNPs and in the presence of SAL, Ce6 efficiently produces ROS in a light dose-dependent manner.

Among ROS, singlet oxygen (1O_2) is the most important species involved in the photo-oxidative cellular damages induced by PDT. Based on this, its production by SAL/Ce6@kVE kNPs was determined by recording the decrease of DMA absorption peak at 378 nm. In fact, DMA is converted to its non-fluorescent endoperoxide derivative in the presence of 1O_2 ; as expected, the solution containing the sole DMA probe did not show any decrease of the 378 nm peak upon irradiation (Fig. 1E); on the other hand, upon irradiation with red light up to 300 s, the solution containing SAL/Ce6@kVE kNPs and DMA produced a gradual decrease of DMA absorbance, confirming that singlet oxygen production is light-dose dependent and ascribable to the presence of Ce6. It is worth to note that, the presence of VE acetate in SAL/Ce6@kVE did not negatively affect both singlet oxygen both ROS production. In fact, the profile of DMA photooxidation in the presence of Ce6/SAL@kVE (Fig. 1E) was absolutely comparable with those of Ce6 loaded kNPs prepared in the absence (Ce6@ker) and in the presence of VE acetate (Ce6@kVE) (Fig. S5). Similarly, the total amount of ROS produced after NPs irradiation with red light was comparable between SAL/Ce6@kVE (Fig. 1D) and Ce6@kVE and Ce6@ker (Fig. S6), thus excluding any ROS scavenging capability of VE as well as any negative effect on PDT efficiency.

3.2. Cytotoxicity of SAL-loaded kNPs toward differentiated and CSCs

The *in vitro* cytotoxic activity of SAL-loaded kNPs toward breast adenocarcinoma MCF-7 cells and triple negative MDA-MB-231 cells grown as monolayers was evaluated and compared with free SAL. Cells were incubated with increasing concentrations of drug/kNPs (up to 20 μ M SAL) and incubation times (up to 72 h), and cell viability was assessed by the MTS assay. Our results indicate that SAL cytotoxicity is

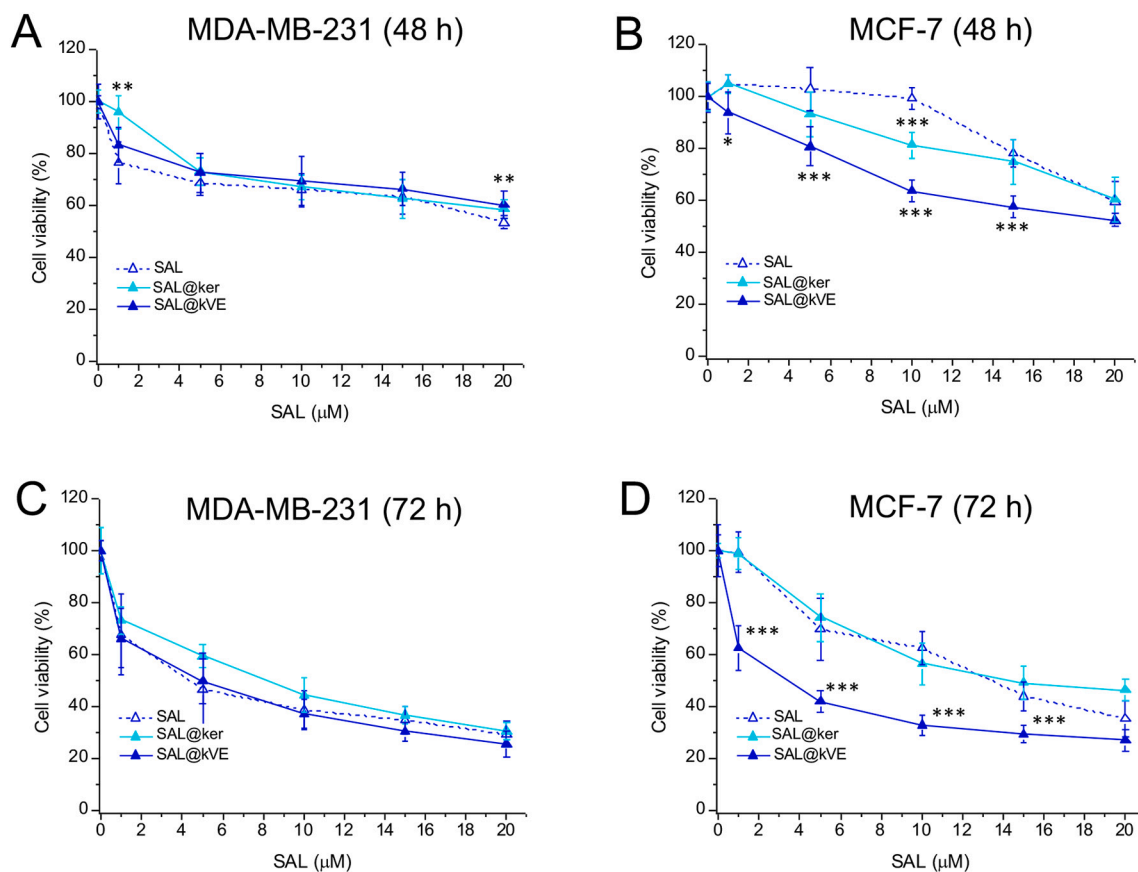


Fig. 2. Cytotoxicity of SAL formulations toward monolayered differentiated cells. Cytotoxicity curves of MDA-MB-231 (A, C) and MCF-7 (B, D) cells exposed to increasing concentration of free SAL, SAL@ker, SAL@kVE for 48 h (A, B) and 72 h (C, D), and assessed for viability with the MTS assay at the end of the incubation time. Data are expressed as mean \pm SD of at least two independent experiments carried out in triplicate. * $p < 0.05$; ** $p < 0.01$; *** $p < 0.001$ significantly different from SAL free (Student's *t*-Test).

dependent on incubation time (Figs. 2 and S7): the exposure of cells to SAL formulations for 24 h did not considerably affect cells viability, with a maximum 20% mortality measured in both cell lines (Fig. S7 A,B), while at the highest concentration tested and with longer incubation times, *i.e.* 48 h and 72 h (Fig. 2A–D), the extent of cells mortality significantly increased.

Notably, the two cell lines displayed different responsiveness to the different SAL formulations both in terms of cytotoxic profiles and IC₅₀ values. In MDA-MB-231 cells (Fig. 2A and C), viability curves were rather superimposable with IC₅₀ values at 72 h of 4.29, 8.03 and 4.95 μ M for SAL, SAL@ker kNPs and SAL@kVE kNPs, respectively. In MCF-7 cells (Fig. 2B and D), SAL@kVE kNPs (IC₅₀ at 72 h = 3.38 μ M) were significantly more effective than SAL (IC₅₀ at 72 h = 13.26 μ M) and SAL@ker kNPs (IC₅₀ at 72 h = 14.02 μ M). To exclude any possible contribution of VE acetate on the superior cytotoxicity induced by SAL@kVE kNPs, cells were incubated with VE acetate at the same concentration of the corresponding kNPs. Results showed a slight viability reduction (~20%) exclusively in MCF-7 cells regardless of the concentration tested (Fig. S7C), indicating that VE acetate is well tolerated by cells and that its use as aggregating agent for kNPs preparation is safe.

Based on these preliminary results, the subsequent experiments were performed using only free SAL and SAL@kVE kNPs, being the latter the most potent SAL nanoformulation.

The efficacy of SAL@kVE kNPs against CSCs was assessed by using the mammosphere model, *i.e.* tridimensional cells cultures of breast cancer cells enriched in CSCs [55]. First generation mammospheres were incubated with SAL or SAL@kVE kNPs for 48 h or 72 h; at the end of the incubation time, mammospheres were disaggregated and re-seeded to form the 2nd generation of mammospheres. The capability of SAL to affect spheres formation, measured as mammosphere formation efficiency (MFE), was comparable between the two formulations (Figs. 3 and S8), while a different extent of MFE reduction was observed among the two cell lines. In fact, while MFE reduction was concentration-dependent in MDA-MB-231 cells (Fig. 3A), the MFE of MCF-7 mammospheres was below 50%, irrespective to SAL concentration and incubation time (Fig. 3B). These results demonstrate that, conversely to what observed in monolayered cells, MCF-7 line cultured as tridimensional and CSC-enriched model is significantly more sensitive to SAL and SAL@kVE kNP treatment. Altogether these results demonstrate that the delivery of SAL in kNPs does not alter the antitumoral profile of SAL *in vitro*.

3.3. Cytotoxicity of SAL/Ce6@kVE kNPs combined treatment toward differentiated and CSCs

SAL, either as free drug or loaded into kNPs, proved to be capable of killing differentiated cancer cells and reducing the capability of mammosphere formation as a parameter of stemness reduction. However, the concentration of SAL required to kill 50% of cells (IC₅₀) is not compatible with clinical translation and, most importantly, none of the tested concentrations and exposure times allowed reaching complete cell death. To address this issue, we explored the combination of SAL cytotoxicity and Ce6-PDT. For *in vitro* combination therapy, monolayered cells were treated for 48 h with either single or combined drugs, delivered in standard solvents or loaded into kNPs (Ce6 and SAL loaded in NPs in the 1:1.4 molar ratio), and irradiated with red light before assessing cells viability 24 h post-PDT (Fig. 4A–B).

For mono-therapy treatments, each single drug delivered by kNPs is significantly more effective in inducing cell mortality than the respective free drug (Table S6), except SAL@kVE kNPs in MDA-MB-231 cells. According to the results shown in Fig. 2, the IC₅₀ values measured for SAL and SAL@kVE kNPs significantly varied within the two cell lines (~30 μ M in MCF-7 vs. 10 μ M in MDA-MB-231). The dose-response curves of cells not exposed to light (*i.e.* dark cytotoxicity) confirmed the negligible cytotoxicity of Ce6 formulations in both cell lines

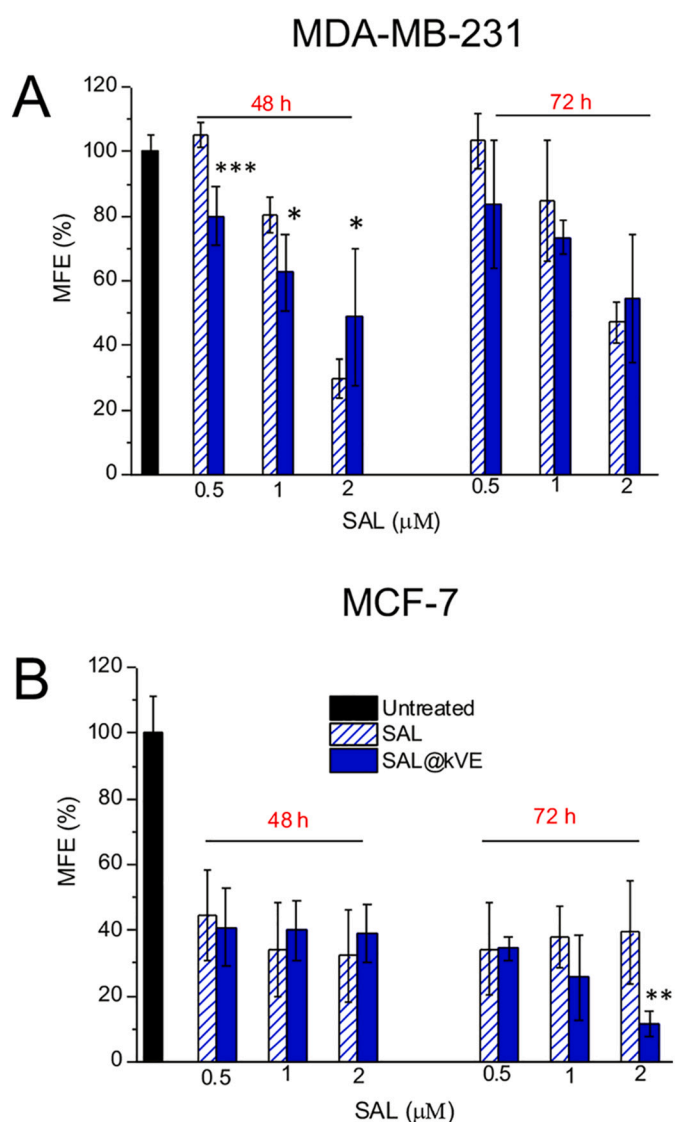


Fig. 3. Percentage Mammosphere Formation Efficiency (MFE) in MDA-MB-231 (A) and MCF-7 (B) derived 2nd generation mammospheres obtained from 1st generation mammospheres treated for 48 or 72 h with free SAL or SAL@kVE and re-seed in non-adherent conditions. MFE was evaluated after 7 and 4 days from the re-seeding for MCF-7 and MDA-MB-231, respectively. Data are expressed as mean \pm SD of at least two independent experiments carried out in triplicate. * $p < 0.05$; ** $p < 0.01$; *** $p < 0.001$ significantly different from SAL free (Student's *t*-Test).

(Fig. S9A–B). Notably, while the effect of SAL in MDA-MB-231 cells was comparable irrespective the drug delivery vehicle and the drugs combination, SAL cytotoxicity in MCF-7 cells was significantly improved when delivered through kNPs, and for all combinations. This result could be ascribed to a different internalization behavior of drugs in kNPs compared to free drugs. Indeed, the two cell lines displayed a different capability of drug/kNP uptake (Fig. S9C) when comparing free Ce6 and Ce6@kVE kNPs: in MDA-MB-231 cells, the intracellular uptake is only slightly, but significantly, increased in the case of Ce6@kVE kNPs; on the other hand, the uptake of the free photosensitizer in MCF-7 cells is reduced by 50% with respect to Ce6@kVE kNPs. This result is in agreement with the different cytotoxicity profiles of Ce6 formulations measured in the two cell lines (Fig. 4A–B) after PDT treatment: the curves of free Ce6 and Ce6@kVE kNPs are rather superimposable in MDA-MB-231 cells, whereas Ce6@kVE kNPs determined a significantly higher cell mortality than that caused by free Ce6 in MCF-7 cells.

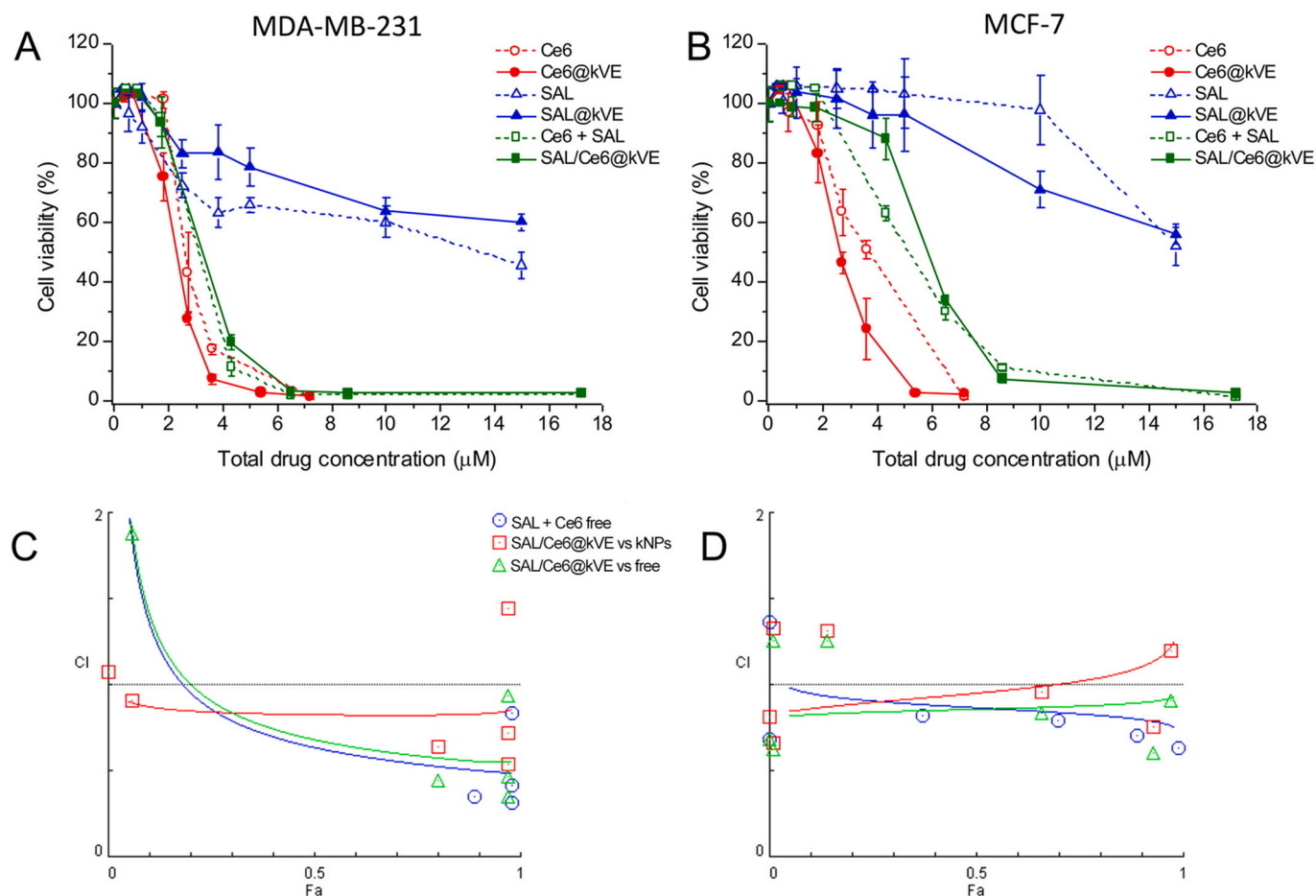


Fig. 4. Cytotoxic profiles of single and combined treatments in differentiated MDA-MB-231 (A, C) and MCF-7 (B, D) cells cultured as monolayers. (A, B) Dose-response curves of cells incubated for 48 h with single drugs or their combination delivered free or in kNPs and irradiated with 20 J/cm^2 of light (when PDT was part of the treatment). After additional 24 h in drug-free medium, cell viability was measured by MTS assay. Total drug concentration is referred to SAL + Ce6 concentration. Data are expressed as mean percentage \pm SD of at least three independent experiments, carried out in triplicate. (C, D) Plots of combination index (CI) vs. fraction affected (Fa) relative to cells treated with Ce6 and SAL in the 1:1.4 molar ratio.

In accordance with our previous results on HeLa cells [33], the current findings confirm that our water-soluble and high-molecular-weight keratin is intrinsically able to enhance the intracellular uptake of Ce6, thus augmenting its effectiveness. Furthermore, results on cells treated with Ce6/SAL drug combinations followed by light irradiation, afforded very similar IC_{50} for all formulations and on both cell lines (Fig. 4A–B, Table S6). Compared to Ce6@kVE and SAL@kVE kNPs, SAL/Ce6@kVE treatment exhibited a synergistic effect between drugs ($\text{CI} < 1$) for all Fa values on MDA-MB-231 cells. On the contrary, when SAL/Ce6@kVE or SAL + Ce6 combination approaches are compared to free drugs monotherapies, drugs interaction was found antagonist ($\text{CI} > 1$) for Fa values lower than 0.2 and synergic for all other Fa values (Fig. 4C). Interestingly, the same analysis performed on MCF-7 cells (Fig. 4D) revealed synergism regardless of the delivery mode. The synergistic interaction between Ce6-PDT and SAL treatment determined favorable dose reduction indices (DRIs), irrespective of the delivery vehicle. Of note, DRI values of 9 and 5 for MCF-7 and MDA-MB-231 cells, respectively were observed for SAL while DRIs for Ce6 showed values in the range 1.2–2.3 (Table S6). These results indicate that the combined treatment significantly improves the overall response even in differentiated cancer cells, which are very poorly susceptible to SAL, thus allowing for a lower SAL dosage.

3.4. Cell death mechanisms analysis

To gain more insight into the factors determining the synergistic

interaction between SAL and Ce6-PDT treatments, and being oxidative stress the main cause of cells death upon PDT treatment as well as one of the biological effects induced by SAL [56,57], we first measured intracellular ROS production after mono- and combined therapies. Fig. 5 reports the total ROS increase measured immediately after cells irradiation and shows that ROS production is substantially lower in MCF-7 cells as compared to MDA-MB-231 cells. In fact, in MCF-7 cells all treatments determined a two-fold increase of ROS content as respect to untreated cells with no significant differences among the different formulations. On the other hand, a ten-fold ROS increment was measured in MDA-MB-231 cells when combination therapy was performed, *i.e.* SAL/Ce6 as free or loaded into kNPs. Interestingly, when both cell lines were incubated with VE acetate at concentration equal to those present in kNPs, no effect on ROS production was observed, thus confirming that, despite its antioxidant potential, VE acetate does not interfere with the treatment modality.

Overall, these findings well correlate with the lower cytotoxicity measured in MCF-7, accounting for a higher drug resistance of this cell line toward SAL monotherapy.

The mechanism of cells death was further analyzed by determining the lactate dehydrogenase (LDH) release, as a measure of necrotic cells death *via* membrane permeabilization (Fig. 6A–B). The percentage of LDH released from cells significantly increases in a dose-dependent manner only upon Ce6-PDT treatment, alone or in combination with SAL. On the other hand, treatment with SAL alone at the highest concentration, *e.g.* $10 \mu\text{M}$, determined a 40% and 20% LDH release in MDA-

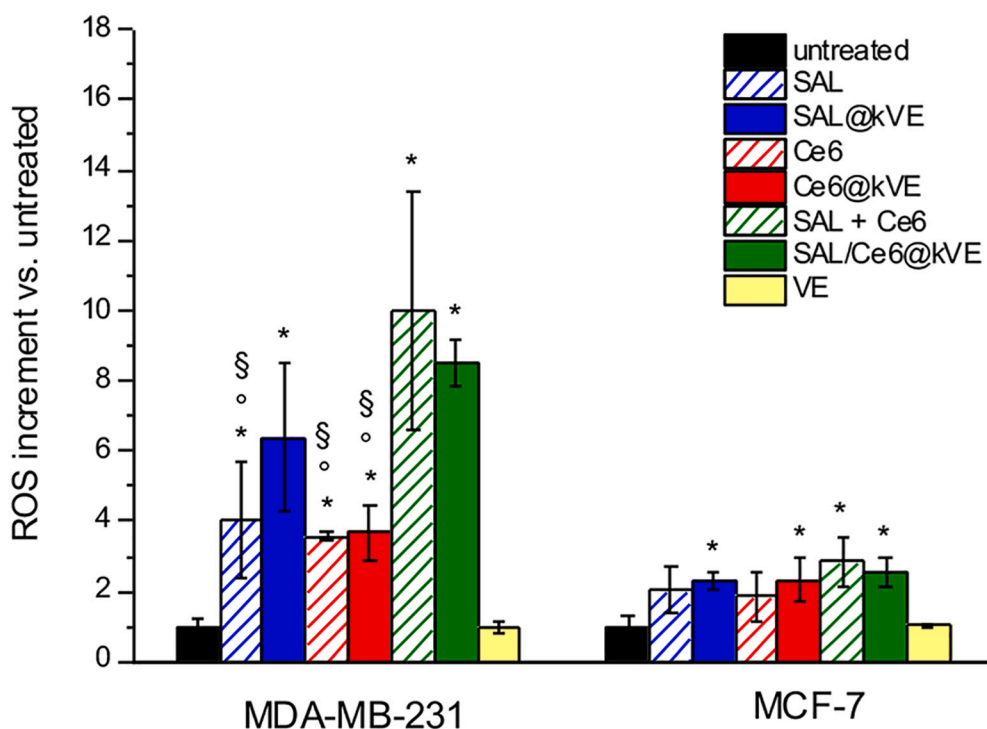


Fig. 5. ROS production after mono- and combined treatments. Differentiated MDA-MB-231 and MCF-7 cells, previously exposed to the different treatments for 48 h, were assessed for ROS analysis by FACS immediately after light exposure. Data are expressed as mean percentage \pm SD of at least two independent experiments, carried out in triplicate. * $p < 0.05$, significantly different from control cells; $^{\circ}p < 0.05$, significantly different from SAL + Ce6; $^{\S}p < 0.05$, significantly different from SAL/Ce6@kVE (one-way ANOVA, Bonferroni's correction).

MB-231 and MCF-7 cells, respectively. Moreover, our results indicate that a lower LDH release is induced when drugs are delivered by kNPs, although this behavior is not reflected in a lower cytotoxicity.

In agreement with literature data [56,58], Annexin V/PI assay (Fig. 6C–D) revealed that apoptosis is the predominant mechanism of SAL-induced death mechanism in MDAMB-231 cells (~40%), whereas it only scarcely activates the apoptotic response in MCF-7 cells (~10%), regardless of the drug delivery mode. It is worth noting that the low apoptotic and necrotic rate observed in MCF-7 cells in our experimental design, well agree with both the low cytotoxicity and oxidative stress previously discussed in the previous sections.

When Ce6-PDT was performed, the percentage of apoptotic cells was very low and similar among the two cells lines (~20% of positive cells). Interestingly, in MDA-MB-231 cells treated with combined free drugs or SAL/Ce6@kVE kNPs, a significant increase of apoptotic cells was detected (~80%), thus indicating an amplified effect on the apoptotic pathway as respect to drugs alone. Collectively, these data represent a preliminary but robust evidence that SAL/Ce6@kVE kNPs plus PDT might be an effective and selective treatment option for triple-negative breast cancer. Indeed, our results account for a significant higher cytotoxic activity of SAL/Ce6@kVE kNPs plus PDT on MDA-MB-231 cells as respect to differentiated MCF-7 cells, being the former a well-established model of human TNBC.

3.5. Combination therapy effect on stemness

It is widely established among the scientific community that, even if CSCs are considered as leading progenitors of tumor masses, also differentiated cancer cells can revert their phenotypes to stem cells in order to preserve the balance between stem and differentiated subpopulations, the so called 'dynamic equilibrium' [59]. Importantly, the present study represents the first attempt tackling the potential role of Ce6-PDT in eradicating CSCs or limiting their stemness potential.

Thus, in order to assess if our dual approach is useful to reduce the stemness potential of differentiated cancer cells, we measured the capability of monolayered cells exposed to the different drugs formulations/therapies to form mammospheres [29]. Our results show that the

reduction of MFE is significantly higher when combination therapy is performed, reaching an almost complete suppression of spheres formation at the highest doses and for both cell lines (Fig. 7A–B). Importantly, when drugs are delivered by kNPs, the percentage of MFE reduction is significantly enhanced with respect to free drugs, and this effect is even more pronounced in the triple negative cell line. It is worth noting that the treatment of cells with VE acetate alone did not affect their aptitude to form mammospheres (yellow bars), thus excluding VE acetate as a possible enhancer of kNPs capability to reduce cancer cells stemness.

Remarkably, this experiment highlights that, especially in the case of combined treatment, the drugs' doses that did not determine an elevated mortality in cell monolayers, are able to limit the cells self-renewal capacity. Moreover, in order to verify if our drugs treatments/formulations were also able to directly kill the CSC population in 1st generation mammospheres, we measured the effect on stemness on the 2nd generation (Fig. 7C–D). The reduction of MFE values in MDA-MB-231 mammospheres was shown to be dependent on drugs concentrations for all treatments, except for SAL formulations where resistance was revealed (Fig. 7C). Conversely to what observed for 1st generation mammospheres (Fig. 7A), the SAL/Ce6@kVE-PDT and the Ce6-PDT were able to completely abolish spheres formation at the highest doses; however, the treatment with SAL/Ce6@kVE kNPs at intermediate doses (e.g. 0.72 μ M Ce6 and 1 μ M SAL), was the most powerful in reducing MFE (Fig. 7C). The same experiment performed on MCF-7 cells (Fig. 7D) confirmed the higher resistance of this cells line not only toward SAL but also to Ce6-PDT treatment alone; indeed, MFE values equal to zero were measured exclusively when combination therapies were performed.

In order to assess if our treatment strategy is successful in terms of CSCs eradication, we focused our experiments on MDA-MB-231 mammospheres. In fact, this cells line forms spheres with a higher CSCs percentage as respect to MCF-7 cells [29], thus constituting a more representative model for our purpose. Second generation MDA-MB-231 mammospheres displayed a significant CSC reduction as respect to untreated mammospheres for all treatments groups (Fig. S10A); furthermore, in agreement with results shown in Fig. 7C (SAL 1 μ M, Ce6 0.72 μ M), the combined therapy, regardless of the drug delivery modality,

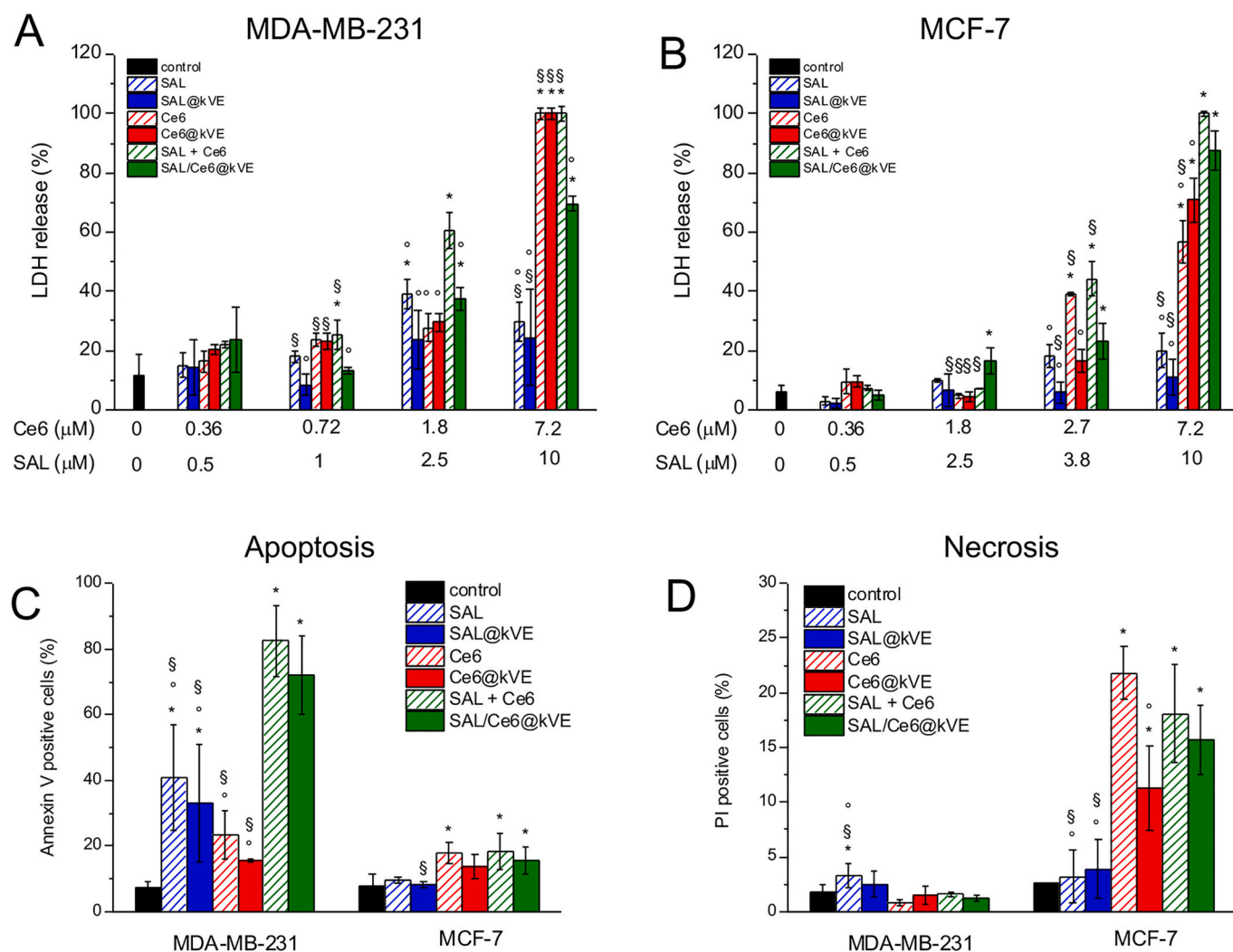


Fig. 6. Analysis on the mechanisms of cell death after single and combined treatments in differentiated MDA-MB231 and MCF-7 cells. Percentage of LDH released in the culture medium of MDA-MB-231 (A) and MCF-7 (B) cells incubated for 48 h with the different drugs/therapies, exposed to light irradiation (20 J/cm^2) and released in drug-free medium for additional 24 h before assay performing. Percentages of apoptotic (C) and necrotic (D) cells measured by the Annexin V/PI assay in cells incubated for 48 h with the different drugs/therapies (SAL dose $1 \mu\text{M}$, Ce6 dose $0.72 \mu\text{M}$), exposed to light and released in drug-free medium for additional 24 h. Data are expressed as mean percentage \pm SD of at least two independent experiments, carried out in triplicate. * $p < 0.05$, significantly different from control cells; $^\circ p < 0.05$, significantly different from SAL + Ce6; $^\S p < 0.05$, significantly different from SAL/Ce6@kVE kNPs (one-way ANOVA, Bonferroni's correction).

was the most powerful against CSCs, inducing an almost complete cells eradication (0.55 and 0.65 residual CSCs after SAL/Ce6@kVE kNPs and SAL + Ce6 treatment, respectively). Interestingly, while in the mammospheres formation experiment, we observed greater MFE reduction for Ce6-PDT as respect to SAL monotherapy (Fig. 7 C), the ALDH assay revealed that the activity of SAL against CSC eradication is maintained, with only 2.25 and 1.65% residual CSCs for SAL and SAL@kVE kNPs treatments, respectively. Thus, since in our mammospheres model the majority of cells are differentiated, we can speculate that SAL treatment is primarily effective toward CSCs whereas the remaining cells are probably more refractory and tend to develop resistance. On the other hand, Ce6-PDT seems to be equally effective, in a dose dependent manner, toward both differentiated cells and CSCs.

In order to assess if the higher drugs' ability (alone or combined) to reduce MFE values when delivered through kNPs could be attributed to a different uptake profile, we analyzed the Ce6 distribution in the 1st generation of MDA-MB-231 mammospheres. As shown in Fig. S10B, Ce6 fluorescence is significantly higher when formulated into kNPs as respect to the free form, as evident by the representative median plane images and the maximum projection images obtained by the superimposition of 20 different focal planes. Moreover, looking at the extent of

PS penetration inside the mammospheres' inner core, while free Ce6 remains confined in the outer rims of cells, its delivery with kNPs allows a more homogeneous distribution throughout the cellular structure. This key result, besides confirming the superior uptake already observed in cells monolayer (Fig. S5C), indicates the capability of our system to improve drug availability and drug penetration in the inner part of the malignancy, where CSCs are usually located.

3.6. *In vivo* experiments on zebrafish embryos

In order to verify whether the activity of SAL@kVE kNPs is preserved also in living organisms, zebrafish was employed as the *in vivo* model to analyze the interference of the drug with the Wnt/ β -catenin signaling [52], one of the best known pathways modulated by SAL both *in vitro* and *in vivo* [60,61]. To this purpose, transgenic reporter zebrafish lines expressing a GFP under the control of a Wnt responsive promoter (Tg (7xTCFX.lasiam:EGFP)) [62] were treated with SAL and SAL@kVE kNPs. As preliminary test, SAL or SAL@kVE kNPs ($1 \mu\text{M}$ SAL) were added to the fish water of ~ 12 hours post fertilization (hpf) embryos. After 15 h of treatment (embryos at ~ 27 hpf), the effect of SAL on the reporter gene was analyzed (Fig. S11), demonstrating that GFP

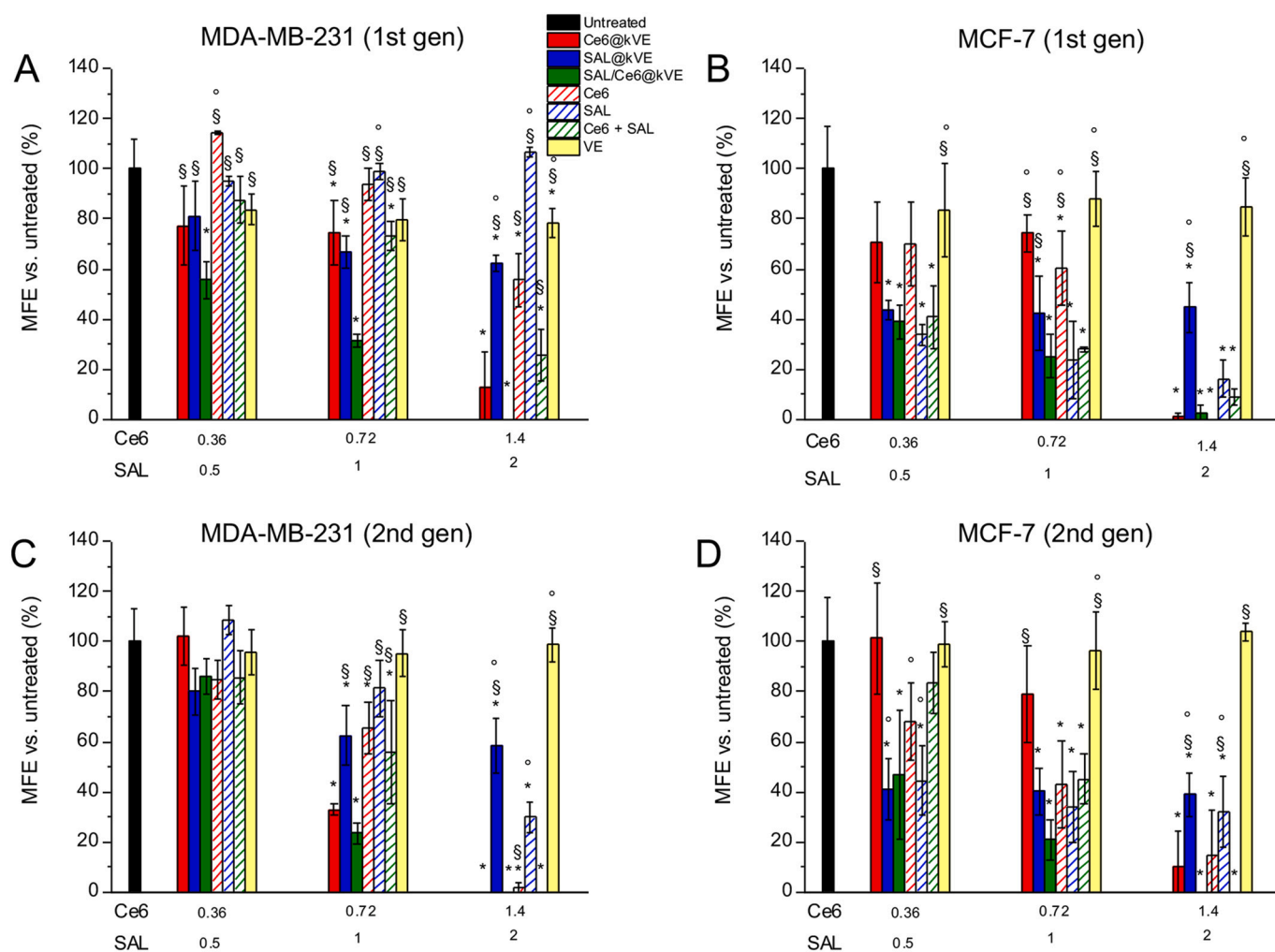


Fig. 7. Mammosphere formation efficiency (MFE) after single and combined treatments. Percentage MFE measured in 1st generation mammospheres generated from MDA-MB-231 (A) and MCF-7 (B) monolayered cells incubated for 48 h with the free drugs or with the nanoformulations, irradiated with 20 J/cm², and re-seeded in non-adherent conditions to allow formation of spheres. Percentage MFE measured in 2nd generation mammospheres generated from 1st generation mammospheres of MDA-MB-231 (C) and MCF-7 (D) exposed to drugs for 48 h, irradiated with 1 J/cm², and immediately re-seeded in non-adherent conditions. MFE was evaluated after 7 and 4 days from the re-seeding for MCF-7 and MDA-MB-231, respectively. Data are expressed as mean \pm S.D. of at least two independent experiments, carried out in triplicate. **p* < 0.05, significantly different from control cells; °*p* < 0.05, significantly different from SAL + Ce6; §*p* < 0.05, significantly different from SAL/Ce6@kVE kNPs (one-way ANOVA, Bonferroni's correction).

fluorescence was similarly reduced in SAL and SAL@kVE kNPs treated animals as respect to controls. Moreover, as previously reported for SAL [62] and in accordance with reduced Wnt signaling, the sagittal axis of the larvae was shortened in comparison to the control animals (Fig. S7B), thus supporting the proof of concept on the efficacy of SAL-loaded kNPs in a living organism.

To further assess the effect on stemness of our delivery system in a more complex experimental model, all different kNPs formulations were injected directly *in vivo* in the yolk of zebrafish fertilized eggs at one cell stage. The experiments were performed in heterozygous Tg(7xTCFX.lasiam:EGFP), and the effects of the treatments were observed 25–27 h later, when the body plan of the organism is already formed and the Wnt/ β -catenin phenotype is clearly identifiable. It is worth to note that, even if the proposed *in vivo* model did not represent a canonical model for cancer disease, it well represents a model of stemness.

Thus, when sublethal concentrations of SAL were injected in Wnt-GFP cells, SAL@kVE kNPs significantly decrease GFP fluorescence with respect to controls, while the same dose of free SAL did not, confirming again that the delivery of SAL nanoformulations improve pharmacological potential against the Wnt/ β -catenin signaling pathways (Fig. 8), Tg(7xTCFX.lasiam:EGFP) line), thus limiting cell

stemness. Importantly, the capability of SAL to modulate Wnt was maintained even when SAL/Ce6@kVE kNPs were injected in the embryos, while Ce6@kVE kNPs not activated with light did not decrease GFP fluorescence. As a further proof of the specificity of the interaction of SAL with the Wnt promoter, when the same drug formulations were injected in the housekeeping GFP line Tg(hsa.cox8a:mls-EGFP) (Fig. 8) no effects on basal GFP fluorescence were observed.

4. Conclusions

We have reported the unprecedented, highly reproducible and facile in-water preparation of keratin-based nanoformulations loaded with salinomycin and chlorin e6 using vitamin E acetate as aggregating agent, thus avoiding the use of toxic solvents and cross-linking agents to induce nanoparticle formation and stabilization. SAL/Ce6@kVE kNPs were prepared with a Ce6/SAL ratio of 1:1.4 (w/w) to investigate whether the combination of the anti-CSC activity of SAL with Ce6-based PDT was able to simultaneously eradicate differentiated cells and stem cells in breast cancer models. *In vitro* cytotoxicity studies highlight a synergistic effect of the SAL/Ce6 combination in MDA-MB-231 and MCF-7 cell lines, enabling a significant dose reduction for SAL; however, MCF-7

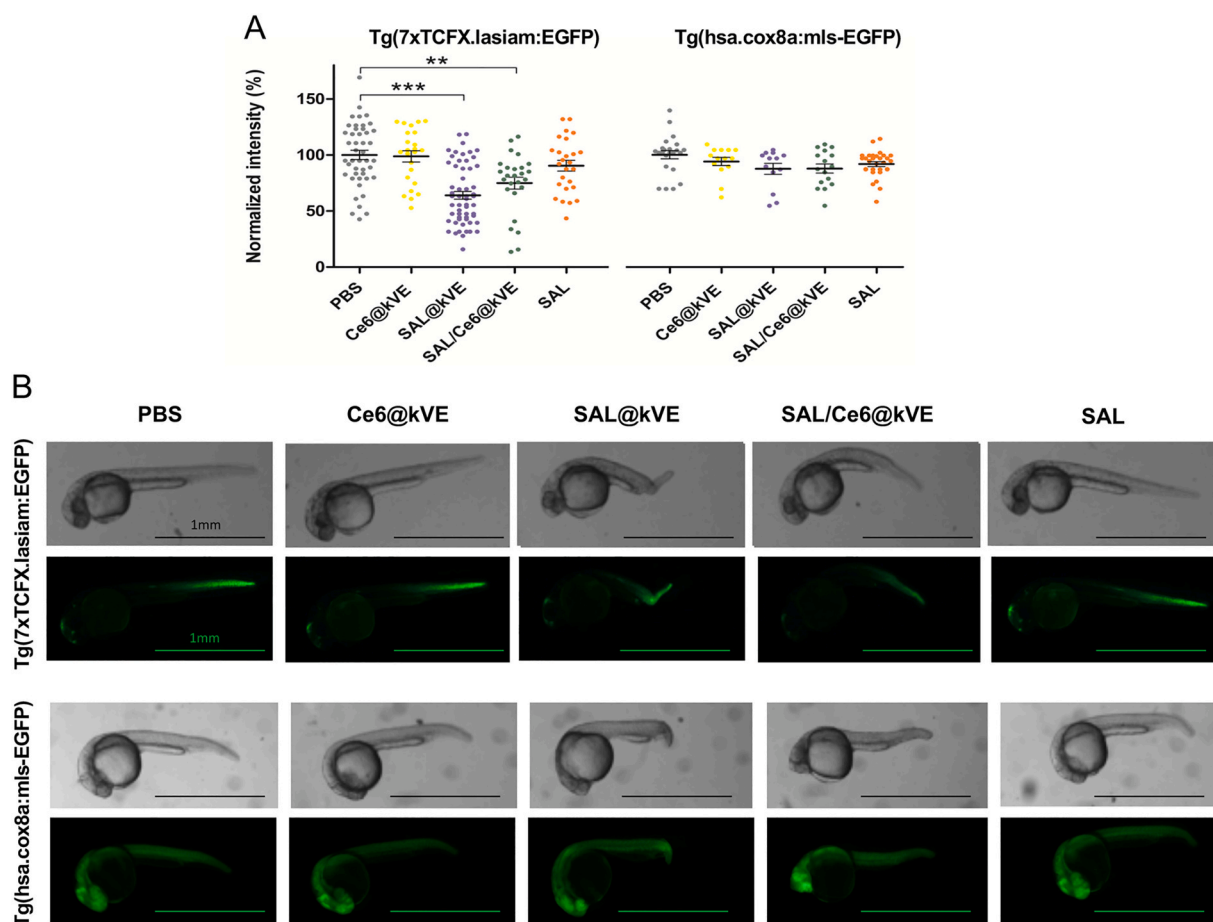


Fig. 8. *In vivo* analysis of SAL interference with the Wnt- β catenin signaling pathways measured in zebrafish embryos microinjected at one-cell stage with the different drug formulations. The analysis was performed in parallel on GFP fluorescent zebrafish Wnt-dependent reporter fishes (line Tg(7xTCFX.lasiam:EGFP)) and on Wnt-independent GFP fluorescent ubiquitous gene reporter fishes (line Tg(hsa.cox8a:mls-EGFP)). All embryos were microinjected with PBS, SAL, SAL@kVE, SAL/Ce6@kVE, and Ce6@kVE kNPs (SAL dose 0.05 pmol). A) Fluorescence quantification (means \pm SEM) derived from fluorescence images of embryos; dots represent zebrafish embryos treated for each condition. B) Representative bright-field and epifluorescence microscopy images of treated embryos; Scale bars: 1 mm.

cells have proved to be more resistant to the combined treatment, displaying higher IC_{50} , lower ROS production and lower activation of the apoptotic response. Sub-lethal concentrations of drugs, especially when combined and loaded into kNPs, are able to reduce the stemness of differentiated BC cells and inhibit the formation of CSC-enriched mammospheres, highlighting the potential of this combination therapy in limiting self-renewal and eradicating CSCs. The higher efficacy of SAL/Ce6@kVE kNPs compared to standard treatments may be related to the enhancement of drug penetration into the inner mammosphere region. *In vivo* investigations on zebrafish embryos reveal that SAL-loaded kNPs were able to interfere with the Wnt/ β -catenin signaling pathway, confirming that kNPs do not alter the CSC-specific cytotoxic activity of SAL also in a living model organism. Based on these observations, SAL/Ce6@kVE kNPs represent an important breakthrough to target breast cancer cells as well as CSCs, thus providing a valuable strategy for the treatment of triple negative breast cancer. From a translational point of view, further experiments need to be performed in pre-clinical animal models to confirm that the effects and the molecular pathways involved are conserved.

CRediT authorship contribution statement

Francesca Moret: Conceptualization, Methodology, Supervision, Data analysis, Writing and Editing **Greta Varchi:** Conceptualization, Methodology, Original draft preparation, Editing; **Greta Avancini:** *In vitro* experiments, Data analysis **Andrea Guerrini:** Conceptualization,

Nanoparticles preparation **Claudia Ferroni:** Nanoparticles characterization, Data analysis, Editing **Daniele Tedesco:** Nanoparticles characterization, Data analysis, Editing **Marco Ballestri:** Nanoparticles characterization, Data analysis **Marta Columbaro:** Nanoparticles characterization (TEM), Data analysis, Editing **Luca Menilli:** *In vitro* experiments on cell death mechanisms, ROS and singlet oxygen experiments, Data analysis, Editing **Elena Reddi:** Editing **Roberto Costa:** *In vivo* experiments, Data analysis **Luigi Leanza:** *In vivo* experiments conceptualization, Writing and Editing.

Funding sources

This work was supported by the University of Padova to FM (PRID-seed 2018) and by the Italian Association for Cancer Research (AIRC) to LL (MFAG 2019-ID 23271) and to GV (IG16740).

Declaration of competing interest

The authors declare that they have no known competing financial interests or personal relationships that could have appeared to influence the work reported in this paper.

Acknowledgment

We thank the Zebrafish Facility of the Biology Department at the University of Padova for logistic and scientific supports and Professor

Giorgia Miolo (University of Padova, Department of Pharmaceutical and Pharmacological Sciences) for the irradiation apparatus.

Appendix A. Supplementary data

Supplementary data to this article can be found online at <https://doi.org/10.1016/j.msec.2021.111899>.

References

- J. Ferlay, M. Colombet, I. Soerjomataram, C. Mathers, D.M. Parkin, M. Piñeros, A. Znaor, F. Bray, Estimating the global cancer incidence and mortality in 2018: GLOBOCAN sources and methods, *Int. J. Cancer* 144 (2019) 1941–1953, <https://doi.org/10.1002/ijc.31937>.
- T. Reya, S.J. Morrison, M.F. Clarke, I.L. Weissman, Stem cells, cancer, and cancer stem cells, *Nature* 414 (2001) 105–111, <https://doi.org/10.1038/35102167>.
- B. Beck, C. Blanpain, Unravelling cancer stem cell potential, *Nat. Rev. Cancer* 13 (2013) 727–738, <https://doi.org/10.1038/nrc3597>.
- D. Nassar, C. Blanpain, Cancer Stem Cells: Basic Concepts and Therapeutic Implications, *Annu. Rev. Pathol.* 11 (2016) 47–76, <https://doi.org/10.1146/annurev-pathol-012615-044438>.
- L. Yang, P. Shi, G. Zhao, J. Xu, W. Peng, J. Zhang, G. Zhang, X. Wang, Z. Dong, F. Chen, H. Cui, Targeting Cancer Stem Cell Pathways for Cancer Therapy, Springer US, 2020, <https://doi.org/10.1038/s41392-020-0110-5>.
- A.Z. Ayob, T.S. Ramasamy, Cancer stem cells as key drivers of tumour progression, *J. Biomed. Sci.* 25 (2018) 20, <https://doi.org/10.1186/s12929-018-0426-4>.
- A.K. Yadav, N.S. Desai, Cancer Stem Cells: Acquisition, Characteristics, Therapeutic Implications, Targeting Strategies and Future Prospects., *Stem Cell Rev. Reports* 15 (2019) 331–355, <https://doi.org/10.1007/s12015-019-09887-2>.
- S. Müller, T. Cañeque, V. Acevedo, R. Rodriguez, Targeting cancer stem cells with small molecules, *Isr. J. Chem.* 57 (2017) 239–250, <https://doi.org/10.1002/ijch.201600109>.
- J. Jiang, H. Li, E. Qaed, J. Zhang, Y. Song, R. Wu, X. Bu, Q. Wang, Z. Tang, Salinomycin, as an autophagy modulator - a new avenue to anticancer: a review, *J. Exp. Clin. Cancer Res.* 37 (2018) 1–13, <https://doi.org/10.1186/s13046-018-0680-z>.
- A. Huczyński, J. Janczak, M. Antoszczak, J. Wietrzyk, E. Maj, B. Brzezinski, Antiproliferative activity of salinomycin and its derivatives, *Bioorg. Med. Chem. Lett.* 22 (2012) 7146–7150, <https://doi.org/10.1016/j.bmcl.2012.09.068>.
- Y. Zhou, C. Liang, F. Xue, W. Chen, X. Zhi, X. Feng, X. Bai, T. Liang, Salinomycin decreases doxorubicin resistance in hepatocellular carcinoma cells by inhibiting the β -catenin/TCF complex association via FOXO3a activation., *Oncotarget* 6 (2015) 10350–65, [doi:10.18632/oncotarget.3585](https://doi.org/10.18632/oncotarget.3585).
- Q.-L. Tang, Z.-Q. Zhao, J.-C. Li, Y. Liang, J.-Q. Yin, C.-Y. Zou, X.-B. Xie, Y.-X. Zeng, J.-N. Shen, T. Kang, J. Wang, Salinomycin inhibits osteosarcoma by targeting its tumor stem cells, *Cancer Lett.* 311 (2011) 113–121, <https://doi.org/10.1016/j.canlet.2011.07.016>.
- T.T. Mai, A. Hamai, A. Hienzsch, T. Cañeque, S. Müller, J. Wicinski, O. Cabaud, C. Leroy, A. David, V. Acevedo, A. Ryo, C. Ginestier, D. Birnbaum, E. Charafe-Jauffret, P. Codogno, M. Mehrpour, R. Rodriguez, Salinomycin kills cancer stem cells by sequestering iron in lysosomes, *Nat. Chem.* 9 (2017) 1025–1033, <https://doi.org/10.1038/nchem.2778>.
- D. Lu, M.Y. Choi, J. Yu, J.E. Castro, T.J. Kipps, D.A. Carson, Salinomycin inhibits Wnt signaling and selectively induces apoptosis in chronic lymphocytic leukemia cells, *Proc. Natl. Acad. Sci.* 108 (2011) 13253–13257, <https://doi.org/10.1073/pnas.1110431108>.
- W. Lu, Y. Li, Salinomycin suppresses LRP6 expression and inhibits both Wnt/ β -catenin and mTORC1 signaling in breast and prostate cancer cells, *J. Cell. Biochem.* 115 (2014) 1799–1807, <https://doi.org/10.1002/jcb.24850>.
- Y.Z. Fu, Y.Y. Yan, M. He, Q.H. Xiao, W.F. Yao, L. Zhao, H.Z. Wu, Z.J. Yu, M. Y. Zhou, M.T. Lv, S.S. Zhang, J.J. Chen, M.J. Wei, Salinomycin induces selective cytotoxicity to MCF-7 mammosphere cells through targeting the Hedgehog signaling pathway, *Oncol. Rep.* 35 (2016) 912–922, <https://doi.org/10.3892/or.2015.4434>.
- V. Plaks, N. Kong, Z. Werb, The cancer stem cell niche: how essential is the niche in regulating stemness of tumor cells? *Cell Stem Cell* 16 (2015) 225–238, <https://doi.org/10.1016/j.stem.2015.02.015>.
- S.K. Singh, I.D. Clarke, M. Terasaki, V.E. Bonn, C. Hawkins, J. Squire, P.B. Dirks, Identification of a cancer stem cell in human brain tumors, *Cancer Res.* 63 (2003) 5821–5828.
- O.O. Ojo, S. Bhaduria, S.K. Rath, Dose-dependent adverse effects of salinomycin on male reproductive organs and fertility in mice, *PLoS One* 8 (2013), e69086, <https://doi.org/10.1371/journal.pone.0069086>.
- Q. Wang, P. Wu, W. Ren, K. Xin, Y. Yang, C. Xie, C. Yang, Q. Liu, L. Yu, X. Jiang, B. Liu, R. Li, L. Wang, Comparative studies of salinomycin-loaded nanoparticles prepared by nanoprecipitation and single emulsion method, *Nanoscale Res. Lett.* 9 (2014) 1–9, <https://doi.org/10.1186/1556-276X-9-351>.
- D. Leng, J. Hu, X. Huang, W. He, Y. Wang, M. Liu, Promoted delivery of salinomycin to lung cancer through epidermal growth factor receptor aptamers coupled DSPE-PEG2000 Nanomicelles, *J. Nanosci. Nanotechnol.* 18 (2018) 5242–5251, <https://doi.org/10.1166/jnn.2018.15424>.
- G. Irmak, M.G. Öztürk, M. Gümüşderelioğlu, Salinomycin encapsulated PLGA nanoparticles eliminate osteosarcoma cells via inducing/inhibiting multiple signaling pathways: comparison with free salinomycin, *J. Drug Deliv. Sci. Technol.* 58 (2020) 101834, <https://doi.org/10.1016/j.jddst.2020.101834>.
- Y. Cui, Y. Yang, M. Ma, Y. Xu, J. Sui, H. Li, J. Liang, Y. Sun, Y. Fan, X. Zhang, Reductive responsive micelle overcoming multidrug resistance of breast cancer by co-delivery of DOX and specific antibiotic, *J. Mater. Chem. B* 7 (2019) 6075–6086, <https://doi.org/10.1039/c9tb01093a>.
- J. Gao, J. Liu, F. Xie, Y. Lu, C. Yin, X. Shen, Co-delivery of docetaxel and salinomycin to target both breast cancer cells and stem cells by plga/tggs nanoparticles, *Int. J. Nanomedicine* 14 (2019) 9199–9216, <https://doi.org/10.2147/IJN.S230376>.
- J. Zhou, M. Sun, S. Jin, L. Fan, W. Zhu, X. Sui, L. Cao, C. Yang, C. Han, Combined using of paclitaxel and salinomycin active targeting nanostructured lipid carriers against non-small cell lung cancer and cancer stem cells, *Drug Deliv.* 26 (2019) 281–289, <https://doi.org/10.1080/10717544.2019.1580799>.
- J. Wei, J. Sun, Y. Liu, Enhanced targeting of prostate cancer-initiating cells by salinomycin-encapsulated lipid-PLGA nanoparticles linked with CD44 antibodies, *Oncol. Lett.* 17 (2019) 4024–4033, <https://doi.org/10.3892/ol.2019.10050>.
- L. Lin, L. Xiong, Y. Wen, S. Lei, X. Deng, Z. Liu, W. Chen, X. Miao, Active targeting of nano-photosensitizer delivery systems for photodynamic therapy of cancer stem cells, *J. Biomed. Nanotechnol.* 11 (2015) 531–554, <https://doi.org/10.1166/jbn.2015.2090>.
- N. Hodgkinson, C.A. Kruger, H. Abrahamse, Targeted photodynamic therapy as potential treatment modality for the eradication of colon cancer and colon cancer stem cells, *Tumor Biol.* 39 (2017) 1–17, <https://doi.org/10.1177/1010428317734691>.
- E. Gaio, C. Conte, D. Esposito, E. Reddi, F. Quaglia, F. Moret, CD44 Targeting Mediated by Polymeric Nanoparticles and Combination of Chlorine TPCS2a-PDT and Docetaxel-Chemotherapy for Efficient Killing of Breast Differentiated and Stem Cancer Cells In Vitro, *Cancers (Basel)* 12 (2020), [doi:https://doi.org/10.3390/CANCERS12020278](https://doi.org/10.3390/CANCERS12020278).
- S. Kwiatkowski, B. Knap, D. Przystupski, J. Saczko, E. Kędzierska, K. Knap-Czop, J. Kotlińska, O. Michel, K. Kotowski, J. Kulbacka, Photodynamic therapy - mechanisms, photosensitizers and combinations, *Biomed. Pharmacother.* 106 (2018) 1098–1107, <https://doi.org/10.1016/j.biopha.2018.07.049>.
- U. Chilakamarthi, L. Giribabu, Photodynamic Therapy: Past, Present and Future., *Chem. Rec.* 17 (2017) 775–802, <https://doi.org/10.1002/tcr.201600121>.
- A. Busi, A. Aluigi, A. Guerrini, C. Boga, G. Sartor, N. Calonghi, G. Sotgiu, T. Posati, F. Corticelli, J. Fiori, G. Varchi, C. Ferroni, Unprecedented behavior of (9 R)-9-hydroxystearic acid-loaded keratin nanoparticles on cancer cell cycle, *Mol. Pharm.* 16 (2019) 931–942, <https://doi.org/10.1021/acs.molpharmaceut.8b00827>.
- E. Gaio, A. Guerrini, M. Ballestri, G. Varchi, C. Ferroni, E. Martella, M. Columbaro, F. Moret, E. Reddi, Keratin nanoparticles co-delivering Docetaxel and Chlorin e6 promote synergic interaction between chemo- and photo-dynamic therapies, *J. Photochem. Photobiol. B* 199 (2019) 111598, <https://doi.org/10.1016/j.jphotochem.2019.111598>.
- P. Liu, Q. Wu, Y. Li, P. Li, J. Yuan, X. Meng, Y. Xiao, DOX-conjugated keratin nanoparticles for pH-sensitive drug delivery, *Colloids Surf. B: Biointerfaces* 181 (2019) 1012–1018, <https://doi.org/10.1016/j.colsurfb.2019.06.057>.
- Y. Li, J. Lin, X. Zhi, P. Li, X. Jiang, J. Yuan, Triple stimuli-responsive keratin nanoparticles as carriers for drug and potential nitric oxide release, *Mater. Sci. Eng. C* 91 (2018) 606–614, <https://doi.org/10.1016/j.msec.2018.05.073>.
- C. Vineis, A. Varesano, G. Varchi, A. Aluigi, Extraction and Characterization of Keratin from Different Biomasses, in: 2019: pp. 35–76, https://doi.org/10.1007/978-3-030-02901-2_3.
- A. Aluigi, M. Ballestri, A. Guerrini, G. Sotgiu, C. Ferroni, F. Corticelli, M. B. Gariboldi, E. Monti, G. Varchi, Organic solvent-free preparation of keratin nanoparticles as doxorubicin carriers for antitumor activity, *Mater. Sci. Eng. C Mater. Biol. Appl.* 90 (2018) 476–484, <https://doi.org/10.1016/j.msec.2018.04.088>.
- F. Foglietta, G.C. Spagnoli, M.G. Muraro, M. Ballestri, A. Guerrini, C. Ferroni, A. Aluigi, G. Sotgiu, G. Varchi, Anticancer activity of paclitaxel-loaded keratin nanoparticles in two-dimensional and perfused three-dimensional breast cancer models, *Int. J. Nanomedicine* 13 (2018) 4847–4867, <https://doi.org/10.2147/IJN.S159942>.
- E. Martella, C. Ferroni, A. Guerrini, M. Ballestri, M. Columbaro, S. Santi, G. Sotgiu, M. Serra, D.M. Donati, E. Lucarelli, G. Varchi, S. Duchi, Functionalized keratin as nanotechnology-based drug delivery system for the pharmacological treatment of osteosarcoma, *Int. J. Mol. Sci.* 19 (2018) 3670, <https://doi.org/10.3390/ijms19113670>.
- Y. Li, X. Zhi, J. Lin, X. You, J. Yuan, Preparation and characterization of DOX loaded keratin nanoparticles for pH/GSH dual responsive release, *Mater. Sci. Eng. C* 73 (2017) 189–197, <https://doi.org/10.1016/j.msec.2016.12.067>.
- A. Aluigi, G. Sotgiu, C. Ferroni, S. Duchi, E. Lucarelli, C. Martini, T. Posati, A. Guerrini, M. Ballestri, F. Corticelli, G. Varchi, Chlorin e6 keratin nanoparticles for photodynamic anticancer therapy, *RSC Adv.* 6 (2016) 33910–33918, <https://doi.org/10.1039/C6RA04208B>.
- N. Duhem, F. Danhier, V. Préat, Vitamin E-based nanomedicines for anti-cancer drug delivery, *J. Control. Release* 182 (2014) 33–44, <https://doi.org/10.1016/j.jconrel.2014.03.009>.
- F. Danhier, T.T.B. Khoué, N. Duhem, B. Ucakar, A. Staub, N. Draoui, O. Feron, V. Préat, Vitamin E-based micelles enhance the anticancer activity of doxorubicin, *Int. J. Pharm.* 476 (2014) 9–15, <https://doi.org/10.1016/j.ijpharm.2014.09.028>.
- V.O. Melnikova, L.N. Bezdetsnaya, D. Brault, A.Y. Potapenko, F. Guillemin, Enhancement of meta-tetrahydroxyphenylchlorin-sensitized photodynamic treatment on human tumor xenografts using a water-soluble vitamin E analogue,

- Trolox, *Int. J. Cancer* 88 (2000) 798–803, [https://doi.org/10.1002/1097-0215\(20001201\)88:5<798::AID-IJC18>3.0.CO;2-8](https://doi.org/10.1002/1097-0215(20001201)88:5<798::AID-IJC18>3.0.CO;2-8).
- [45] E.S.A.M. Al-Sherbini, A.H. El Noury, M.N. El Roubly, T. Ibrahim, Vitamin E (α -tocopherol) enhances the PDT action of hematoporphyrin derivatives on cervical cancer cells, *Med. Laser Appl.* 24 (2009) 65–73, <https://doi.org/10.1016/j.mla.2008.11.004>.
- [46] G. Dusi, V. Gamba, Liquid chromatography with ultraviolet detection of lasalocid, monensin, salinomycin and narasin in poultry feeds using pre-column derivatization, *J. Chromatogr. A* 835 (1999) 243–246, [https://doi.org/10.1016/S0021-9673\(99\)00044-8](https://doi.org/10.1016/S0021-9673(99)00044-8).
- [47] D.S. Liang, J. Liu, T.X. Peng, H. Peng, F. Guo, H.J. Zhong, Vitamin E-based redox-sensitive salinomycin prodrug-nanosystem with paclitaxel loaded for cancer targeted and combined chemotherapy, *Colloids Surf. B: Biointerfaces* 172 (2018) 506–516, <https://doi.org/10.1016/j.colsurfb.2018.08.063>.
- [48] R.W. Korsmeyer, R. Gurny, E. Doelker, P. Buri, N.A. Peppas, Mechanisms of solute release from porous hydrophilic polymers, *Int. J. Pharm.* 15 (1983) 25–35, [https://doi.org/10.1016/0378-5173\(83\)90064-9](https://doi.org/10.1016/0378-5173(83)90064-9).
- [49] P.L. Ritger, N.A. Peppas, A simple equation for description of solute release I. Fickian and non-fickian release from non-swelling devices in the form of slabs, spheres, cylinders or discs, *J. Control. Release* 5 (1987) 23–36. doi:[https://doi.org/10.1016/0168-3659\(87\)90034-4](https://doi.org/10.1016/0168-3659(87)90034-4).
- [50] T.C. Chou, Theoretical basis, experimental design, and computerized simulation of synergism and antagonism in drug combination studies, *Pharmacol. Rev.* 58 (2006) 621–681, <https://doi.org/10.1124/pr.58.3.10>.
- [51] E. Gaio, C. Conte, D. Esposito, G. Miotto, F. Quaglia, F. Moret, E. Reddi, Co-delivery of Docetaxel and Disulfonate Tetraphenyl Chlorin in One Nanoparticle Produces Strong Synergism between Chemo- and Photodynamic Therapy in Drug-Sensitive and -Resistant Cancer Cells, *Mol. Pharm.* (2018) *acs.molpharmaceut.8b00597*. doi: <https://doi.org/10.1021/acs.molpharmaceut.8b00597>.
- [52] E. Moro, G. Ozhan-Kizil, A. Mongera, D. Beis, C. Wierzbicki, R.M. Young, D. Bournele, A. Domenichini, L.E. Valdivia, L. Lum, C. Chen, J.F. Amatruda, N. Tiso, G. Weidinger, F. Argenton, In vivo Wnt signaling tracing through a transgenic biosensor fish reveals novel activity domains, *Dev. Biol.* 366 (2012) 327–340, <https://doi.org/10.1016/j.ydbio.2012.03.023>.
- [53] L. Martorano, M. Peron, C. Laquatra, E. Lidron, N. Facchinello, G. Meneghetti, N. Tiso, A. Rasola, D. Ghezzi, F. Argenton, The zebrafish orthologue of the human hepatocerebral disease gene MPV17 plays pleiotropic roles in mitochondria., *Dis. Model. Mech.* 12 (2019). doi:<https://doi.org/10.1242/dmm.037226>.
- [54] M. Usacheva, S.K. Swaminathan, A.R. Kirtane, J. Panyam, Enhanced photodynamic therapy and effective elimination of cancer stem cells using surfactant–polymer nanoparticles, *Mol. Pharm.* 11 (2014) 3186–3195, <https://doi.org/10.1021/mp5003619>.
- [55] R. Wang, Q. Lv, W. Meng, Q. Tan, S. Zhang, X. Mo, X. Yang, Comparison of mammosphere formation from breast cancer cell lines and primary breast tumors, *J. Thorac. Dis.* 6 (2014) 829–837, <https://doi.org/10.3978/j.issn.2072-1439.2014.03.38>.
- [56] K.Y. Kim, K. Il Park, S.H. Kim, S.N. Yu, D. Lee, Y.W. Kim, K.T. Noh, J.Y. Ma, Y.K. Seo, S.C. Ahn, Salinomycin induces reactive oxygen species and apoptosis in aggressive breast cancer cells as mediated with regulation of autophagy, *Anticancer Res.* 37 (2017) 1747–1758. doi:[10.21873/anticancer.11507](https://doi.org/10.21873/anticancer.11507).
- [57] E. Xipell, M. Gonzalez-Huarriz, J.J. Martinez de Irujo, A. García-Garzón, F.F. Lang, H. Jiang, J. Fueyo, C. Gomez-Manzano, M.M. Alonso, Salinomycin induced ROS results in abortive autophagy and leads to regulated necrosis in glioblastoma., *Oncotarget* 7 (2016) 30626–41. doi:[10.18632/oncotarget.8905](https://doi.org/10.18632/oncotarget.8905).
- [58] Y. Al Dhaheri, S. Attoub, K. Arafat, S. Abuqamar, A. Eid, N. Al Faresi, R. Itratni, Salinomycin induces apoptosis and senescence in breast cancer: upregulation of p21, downregulation of survivin and histone H3 and H4 hyperacetylation, *Biochim. Biophys. Acta* 1830 (2013) 3121–3135, <https://doi.org/10.1016/j.bbagen.2013.01.010>.
- [59] M.K. Jolly, T. Celià-Terrassa, Dynamics of Phenotypic Heterogeneity Associated with EMT and Stemness during Cancer Progression, *J. Clin. Med.* 8 (2019). doi: <https://doi.org/10.3390/jcm8101542>.
- [60] J. Mao, S. Fan, W. Ma, P. Fan, B. Wang, J. Zhang, H. Wang, B. Tang, Q. Zhang, X. Yu, L. Wang, B. Song, L. Li, Roles of Wnt/ β -catenin signaling in the gastric cancer stem cells proliferation and salinomycin treatment, *Cell Death Dis.* 5 (2014) e1039, <https://doi.org/10.1038/cddis.2013.515>.
- [61] F. Wang, L. He, W.-Q. Dai, Y.-P. Xu, D. Wu, C.-L. Lin, S.-M. Wu, P. Cheng, Y. Zhang, M. Shen, C.-F. Wang, J. Lu, Y.-Q. Zhou, X.-F. Xu, L. Xu, C.-Y. Guo, Salinomycin inhibits proliferation and induces apoptosis of human hepatocellular carcinoma cells in vitro and in vivo, *PLoS One* 7 (2012), e50638, <https://doi.org/10.1371/journal.pone.0050638>.
- [62] R. Costa, R. Peruzzo, M. Bachmann, G.D. Montà, M. Vicario, G. Santinon, A. Mattarei, E. Moro, R. Quintana-Cabrera, L. Scorrano, M. Zeviani, F. Vallese, M. Zoratti, C. Paradisi, F. Argenton, M. Brini, T. Cali, S. Dupont, I. Szabò, L. Leanza, Impaired Mitochondrial ATP Production Downregulates Wnt Signaling via ER Stress Induction, *Cell Rep.* 28 (2019) 1949–1960.e6. doi:<https://doi.org/10.1016/j.celrep.2019.07.050>.